AD-A148 611 INFLOW DUCTING IN HIGH-VOLUME-FLOW SUBSONIC ANECHOIC CHAMBERS(U) PENNSYLVANIA STATE UNIV UNIVERSITY PARK APPLIED RESEARCH LAB L R QUARTARARO 12 OCT 83 1/1

UNCLASSIFIED ARL-TM-83-177 N00024-79-C-6043 F/G 20/1 NL

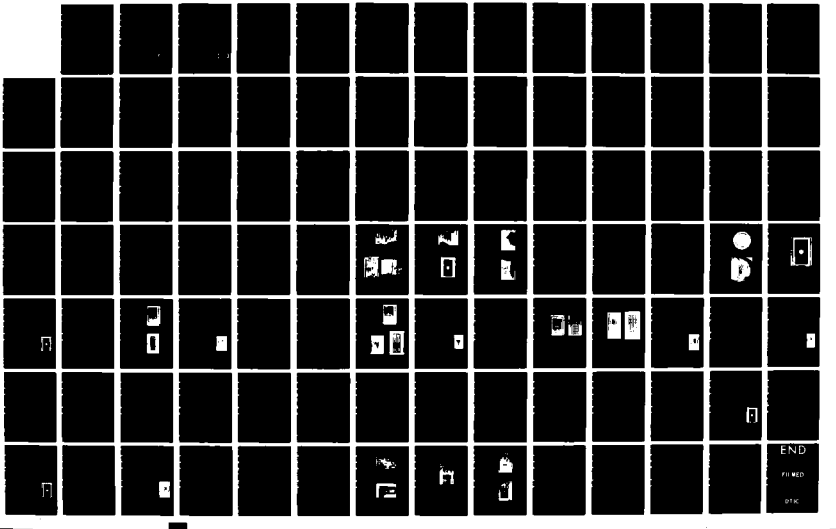

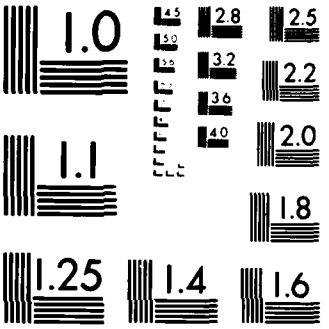

(6)

INFLOW DUCTING IN HIGH-VOLUME-FLOW SUBSONIC ANECHOIC CHAMBERS

Louis Raymond Quartararo

Technical Memorandum
File No. TM 83-177
12 October 1983
Contract N00024-79-C-6043

Copy No. 3

The Pennsylvania State University
Intercollege Research Programs and Facilities
APPLIED RESEARCH LABORATORY
Post Office Box 30
State College, Pa. 16804

NAVY DEPARTMENT

NAVAL SEA SYSTEMS COMMAND

INFLOW DUCTING IN HIGH-VOLUME-FLOW SUBSONIC ANECHOIC CHAMBERS

Louis Raymond Quartararo

Technical Memorandum
File No. TM 83-177
12 October 1983
Contract N00024-79-C-6043

Copy No. 3

The Pennsylvania State University
Intercollege Research Programs and Facilities
Applied Research Laboratory
Post Office Box 30
State College, PA 16804

NAVY DEPARTMENT

NAVAL SEA SYSTEMS COMMAND

Approved for public release

UNCLASSIFIED

SECURITY CLASSIFICATION OF THIS PAGE (When Data Entered)

REPORT DOCUMENTATION PAGE		READ INSTRUCTIONS BEFORE COMPLETING FORM
1. REPORT NUMBER TM 83-177	2. GOVT ACCESSION NO. AD-A148611	3. RECIPIENT'S CATALOG NUMBER
4. TITLE (and Subtitle) INFLOW DUCTING IN HIGH-VOLUME-FLOW SUBSONIC ANECHOIC CHAMBERS		5. TYPE OF REPORT & PERIOD COVERED Technical Memorandum 6. PERFORMING ORG. REPORT NUMBER
7. AUTHOR(s) Louis Raymond Quartararo		8. CONTRACT OR GRANT NUMBER(s) N00024-79-C-6043
9. PERFORMING ORGANIZATION NAME AND ADDRESS Applied Research Laboratory Post Office Box 30 State College, PA 16804		10. PROGRAM ELEMENT, PROJECT, TASK AREA & WORK UNIT NUMBERS
11. CONTROLLING OFFICE NAME AND ADDRESS Naval Sea Systems Command, Code NSEA-63R14 Department of the Navy Washington, DC 20362		12. REPORT DATE 12 October 1983 13. NUMBER OF PAGES 93
14. MONITORING AGENCY NAME & ADDRESS(if different from Controlling Office)		15. SECURITY CLASS. (of this report) UNCLASSIFIED 15a. DECLASSIFICATION/DOWNGRADING SCHEDULE

16. DISTRIBUTION STATEMENT (of this Report)

Approved for public release. Distribution unlimited.
Per NAVSEA - 7 November 1983.

17. DISTRIBUTION STATEMENT (of the abstract entered in Block 20, if different from Report)

18. SUPPLEMENTARY NOTES

19. KEY WORDS (Continue on reverse side if necessary and identify by block number)

Flow Facilities -- Anechoic
Anechoic Chambers -- Flow Through
Aeroacoustic Testing
Anechoic Chamber Design

20. ABSTRACT (Continue on reverse side if necessary and identify by block number)

When studying the aeroacoustic performance of fluid moving machinery, spacial and temporal disturbances in the supply flow may induce otherwise nonexistent noise characteristics in the test device. To control these incoming disturbances, inlet screens, honeycombs, and other wind tunnel configurations have been used. To investigate whether an aeroacoustic test facility could be designed which would utilize neither a wind tunnel configuration nor an inlet control structure at the test device

DD FORM 1 JAN 73 1473 EDITION OF 1 NOV 65 IS OBSOLETE

UNCLASSIFIED

SECURITY CLASSIFICATION OF THIS PAGE (When Data Entered)

inlet, a one-sixth-scale model of a proposed high-volume-flow subsonic anechoic chamber was evaluated. An experimental investigation of inlet-flow controlling walls with combined anechoic and aerodynamic capabilities was carried out. Aerodynamic performance was measured in the plane of a proposed test fan rotor. Data from several inlet wall configurations give guidance in the design of inflow ducting configurations for high-volume-flow subsonic anechoic chambers. The results indicate that substantial reduction of axial turbulence intensities and steady-state spacial disturbances can be achieved without degradation of the anechoic capability of the inlet wall. Because inflow control is no longer needed near the test device inlet, the acoustical characteristics of the test device should match those of a free-field device. It is further noted that with the test device inlet open, known disturbance producing devices can be attached if the experimental objectives require such alterations of the inflow.

ABSTRACT

When studying the aeroacoustic performance of fluid moving machinery, spacial and temporal disturbances in the supply flow may induce otherwise nonexistent noise characteristics in the test device. To control these incoming disturbances, inlet screens, honeycombs, and other wind tunnel configurations have been used. To investigate whether an aeroacoustic test facility could be designed which would utilize neither a wind tunnel configuration nor an inlet control structure at the test device inlet, a one-sixth-scale model of a proposed high-volume-flow subsonic anechoic chamber was evaluated. An experimental investigation of inlet-flow controlling walls with combined anechoic and aerodynamic capabilities was carried out. Aerodynamic performance was measured in the plane of a proposed test fan rotor. Data from several inlet wall configurations give guidance in the design of inflow ducting configurations for high-volume-flow subsonic anechoic chambers. The results indicate that substantial reduction of axial turbulence intensities and steady-state spacial disturbances can be achieved without degradation of the anechoic capability of the inlet wall. Because inflow control is no longer needed near the test device inlet, the acoustical characteristics of the test device should match those of a free-field device. It is further noted that with the test device inlet open, known disturbance producing devices can be attached if the experimental objectives require such alterations of the inflow.

TABLE OF CONTENTS

TABLE OF CONTENTS (continued)

LIST OF FIGURES

LIST OF FIGURES (continued)

LIST OF FIGURES (continued)

LIST OF FIGURES (continued)

ACKNOWLEDGMENTS

The research presented in this paper is a product of the efforts of many individuals. I gratefully acknowledge the assistance of my thesis adviser, Dr. Gerald C. Lauchle, who proposed the research task. He directed the research project and provided guidance throughout its duration. Helpful technical discussions concerning the experimental set up were also provided by Dr. Donald E. Thompson and Mr. Basil E. Robbins. I thankfully credit the Operations Department; especially Professor George B. Gurney, Mr. Allen L. Treaster, Mr. Gregory D. Henderson, the model shop crew, and the machine shop staff of the Garfield Thomas Water Tunnel. Their assistance in their many fields of expertise consistently aided the progress of the project. Midway through the project, Professor James H. Prout joined the project and became an essential contributor to the solution of mechanical and electrical problems in the experiment.

This research was conducted in part to fulfill the requirements of a concurrent Master's Degree program in Acoustics and Architectural Engineering. Professor Gifford H. Albright, Dr. Louis F. Geschwindner, and Dr. Jiri Tichy provided encouragement and administrative assistance during the design and approval of the concurrent course of study.

Funding for this project was provided by the U.S. Naval Sea Systems Command through the Applied Research Laboratory's Exploratory and Foundational (E/F) Research Program, which was administered by Dr. Miles T. Pigott.

CHAPTER I

INTRODUCTION

1.1 Anechoic Chambers

An acoustically free-field environment is one in which the direct field from a sound source predominates and the reflected sound field has an amplitude small enough so that it may be neglected. In practice this result is achieved within specified frequency bounds in anechoic chambers. The design of anechoic chambers is well documented (e.g., Beranek, 1946; Duda, 1977), and has not changed significantly since the acceptance of wedge-shaped fiberglass wall linings as proposed by Beranek (1946).

The walls, roof, and floor of an anechoic chamber must serve two purposes: sound absorption and sound transmission loss. For this reason, standard anechoic chamber design utilizes a two-room construction where the outer room provides isolation from external noise sources, and the inner room provides a support system for the sound-absorbing wedge lining. The resulting space between the two rooms can be varied to alter the free-field characteristics of the completed chamber at low frequencies. The low-frequency cutoff of an anechoic chamber is determined by room volume, room dimensions, wedge geometry, wedge material, and the depth of the air space behind the wedges.

1.2 Anechoic Chambers for use in Aeroacoustic Studies

Often it is desired to perform an acoustical evaluation of fan rotors or other devices which are used to move large volumes of air. Acoustical analysis of fluid moving machinery is complicated by the

noise generating effect of the interaction of incoming turbulence with the fan rotor under test. This problem is of particular importance in the case of fluid moving machinery used in aircraft, where the turbulence of incoming air in flight differs substantially from that found in a static, on-ground test situation. In the static case, inflow disturbances created by atmospheric conditions and the ground, as identified by Hanson (1974), produce noise conditions which differ from those in the in-flight case, thereby hindering the acoustical analysis of in-flight conditions when the equipment is tested in a static configuration. The importance of providing a non-distorted inflow to the fan rotor under test is also apparent when considering the use of screens or other obstructions which are designed to intentionally distort the inflow to a test fan rotor.

One method of simulating in-flight inflow conditions is to test the rotor in a wind tunnel. When the acoustical aspects of this type of solution are considered, the result is a wind tunnel facility which has an open-jet section housed in an anechoic chamber. Wind tunnels of this type are the NASA-Lewis 9 x 15 Anechoic Wind Tunnel (Rentz, 1976; Yuska, et al., 1971) and the Naval Ship Research and Development Center, Carderock, Anechoic Flow Facility (Brownell, 1968). A second method is to remove the flow disturbances with a screen and honeycomb configuration placed over the test-rotor inlet. In this case, the inlet and the inlet-flow control device are situated in an anechoic chamber which allows supply air to enter through mufflers or a porous wall arrangement. Chambers of this type are General Electric's CRD Aero/Acoustic Laboratory in Schenectady, New York (Bekofske, et al., 1977), and NASA-Lewis' Anechoic Chamber (Wazyniak, et al., 1977). An

advantage of this method is that it is not necessary to have a wind tunnel in addition to an anechoic test environment, although auxiliary air pumps may oftentimes be required in order to insure design operation of the test rotor. A disadvantage is that the inlet control device prevents the installation of other screens for intentional flow distortion, and may affect acoustical measurements by altering the radiation impedance of the fan rotor.

1.3 High-Volume-Flow Subsonic Anechoic Chambers

In an attempt to combine the best features of the previous systems, the research presented in this thesis focuses on the design of an anechoic chamber with a high-volume-flow inlet wall system for use in subsonic aeroacoustic studies. It is a purpose of this design to eliminate the need for wind tunnel configurations and inlet control devices which obscure the test-rotor inlet. The goal of the present research is to investigate the flow field in the plane of a typical axial flow fan rotor as a function of different inlet wall configurations and to determine whether a significant reduction of flow distortion can be attained through anechoic chamber inlet wall design alteration.

Designing a flow-controlling anechoic chamber which allows significant air-flow rates through it is a task which demands both acoustical and aerodynamic consideration. The most important aerodynamic criterion is that the flow field at the test-fan rotor be free of large-scale turbulence, vorticity, and non-uniform disturbances. The most important acoustic criteria are that the anechoic property of the chamber not be deteriorated, and that noise not be generated by air entering the chamber. The acoustic criteria

are somewhat difficult to satisfy. The second acoustic criterion suggests that the total open inlet area should be large so as to result in low air velocity through the inlet; however, the first acoustic criterion suggests that this total open inlet area be small so that the wedge treatment area is not diminished. Additionally, the inlet system should not introduce a significant head loss to the flow path.

A summary list of the inlet wall design criteria is presented here, with a short discussion of the implications of each:

- Low Inlet Velocity
  - Should be less than 250 fpm (1.27 m/s) to prevent noise generation at the inlet (Knudsen, 1950).
  - This requires a large open inlet area.
- Anechoic Behavior
  - Should have almost 100% coverage by anechoic wedges.
  - This requires that there be no large open inlet areas.
- Low Head Loss
  - This rules out most types of porous materials and fibrous absorbents of high permeability which might have both acoustic and aerodynamic applications.

- Low Turbulence Generation - This requires that there be no sharp edges, sudden expansions, or sudden contractions, encountered by the inlet air stream.
- Ability to Straighten Non-Uniform Flow - This suggests that the inlet ducting may require flow-straightening vanes.
- High Sound Transmission Loss Capability - This is necessary to aid in maintaining an acceptable ambient noise level in the chamber.
- Structural Integrity - The system must be realizable given the typically large scale and small working space between inner and outer room walls of conventional anechoic chambers.

1.4 Design Approach

It was decided to perform an experimental study of inlet walls for high-volume-flow anechoic chambers. A scale-model anechoic chamber with high-volume-flow capability would be designed and fabricated. Its design would be based upon typical anechoic chamber construction, but it would allow different inlet walls to be fastened onto the inner chamber. This scale model would then be used to investigate experimentally the effect of different inflow configurations on the flow-field at a given test-rotor location.

CHAPTER II

DESIGN OF THE EXPERIMENT

2.1 The One-Sixth-Scale Model

2.1.1 Introduction

The Applied Research Laboratory of The Pennsylvania State University (ARL/PSU) is considering the building of a 24' × 34' × 43' (7.3m × 10.4m × 13.1m) anechoic chamber for use in subsonic aero-acoustic studies of fluid moving turbomachinery. The primary test device to be used in this chamber is the ARL/PSU Axial Flow Research Fan (AFRF), shown in Figure 1 and described by Bruce (1972). This research fan can be used to investigate the fundamental mechanisms of axial-flow fan noise generation and unsteady flow. The proposed anechoic chamber must allow air flow at approximately 300 cfs (8.5 m^3/s) which is the maximum flow of the AFRF. An illustration showing the general design concept is presented in Figure 2.

In order to study experimentally the effect of different inflow ducting configurations on the flow field at a test fan rotor, a one-sixth-scale model of the proposed anechoic chamber was constructed. The inlet duct of the model fan was instrumented at the fan rotor plane, and several inlet wall ducting configurations were examined. Acoustical modeling and associated tests were not performed.

The fan-rotor plane was instrumented with three five-hole probes to measure the three time-average velocity components at each of three radial locations, a hot-wire probe oriented to measure axial flow fluctuations at one radial position, and a pitot-static tube for reference velocity and pressure measurements. Previous

investigations have identified large-scale, axial vortices passing through the rotor plane as a discrete-frequency noise-generating mechanism (e.g., Hanson, 1974). These large-scale, axial vortices are steady-state distortions that are typically formed by nearby walls or a ground plane, as opposed to random inlet disturbances which are typically formed by winds (in outdoor facilities) or wakes shed from fan supports, motor mounts, and other geometric irregularities in the vicinity of the fan inlet. The anechoic chamber construction and careful installation of the fan under test will substantially reduce the occurrence of random inlet disturbances, but steady-state disturbances due to nearby walls and inlet duct configurations will persist. The five-hole-probe system measures the steady-state secondary flows and axial velocity at each probe position in the plane of the fan rotor, and provides a map of secondary flows which is useful in identifying the presence of large-scale vortices that may pass through the plane of the fan rotor.

2.1.2 Design of the One-Sixth-Scale Model

2.1.2.1 Reynolds Number Scaling

The one-sixth-scale model chamber was designed using Reynolds number scaling so that dynamic similarity between the model and the full-scale chamber would be maintained. Two Reynolds numbers are involved in the scaling procedure. The first is the Reynolds number at the inlet wall, the second is that for the AFRF. Constraining conditions for scaling were that the model should be of a size which could be easily assembled and worked with, and that it should have air as the fluid medium. It was found to be impossible to maintain the

Reynolds number both at the inlet wall and in the AFRF without having the flow velocity in the scaled-down AFRF become supersonic. Glycerine and water were examined as possible fluid media, but for these cases too, the flow velocity in the AFRF became much too large to be feasible.

The Reynolds number at the inlet wall was assumed to be critical in that this is the primary experimental variable. Also, the inlet wall is the primary turbulence controlling device in the system. Based on inlet wall Reynolds number scaling, a one-sixth-scale model proved to be most convenient, providing a maximum model dimension of less than 10' (3.05m). In this case the model fan provides a flow rate of 50 cfs (1.42 m^3/s). In order to minimize compressibility effects in the scaled-down AFRF, its diameter is scaled so that the maximum flow velocity at the fan rotor plane is approximately 100 fps (30.48 m/s). Thus, the scale diameter of the AFRF is larger than the exact one-sixth-scale size by a factor of three. From the fundamental viewpoint, this has little consequence, because the AFRF may not be the only research fan evaluated in the anechoic facility.

The scaled-down AFRF duct is made of cast acrylic resin with 1/4" (6.4mm) thick walls and its inner diameter is 9 1/2" (21.4cm). A bellmouth was fabricated from expanded polystyrene and fitted to the duct inlet as detailed in Figure 3.

2.1.2.2 Model Construction

Photographs of the completed model are shown in Figures 4 through 9. The 2 x 4 (1.5" x 3.5" or 3.8 cm x 8.9 cm) framing and homosote sheeting model the outer shell of the full scale chamber. The inner

room of the full scale chamber is modeled with steel-angle-reinforced 1/4" (6.4mm) plywood walls that are lined with expanded polystyrene wedges. Great care was taken during the model construction to insure a sealed system. Seams between the homosote sheets are sealed with duct tape, cracks are filled with caulk, and removable parts which join are treated with foam or felt weather stripping. The floor is made of particleboard and is caulked and bolted to the wall sole plate.

The inner room dimensions were chosen as to allow a full-scale 2' (0.61m) access space between the walls of the two rooms; this space also serves as a backing air-space behind the anechoic wedges. A full-scale 4' (1.22m) space is allotted for air conditioning ductwork above the inner room. The model-scale inner room is mounted on a movable platform so that inlet wall design changes can be performed conveniently. In Figure 7, there is no test inlet wall in place and the inside of the inner room, lined with wedges, is visible.

Because of its light weight, low cost, and ability to be easily mounted, the wedges are made of expanded polystyrene, and were cut to shape by the supplier with a hot wire system. The wedges are individually glued to cardboard panels, which are then fastened to the 1/4" (6.4mm) plywood walls using small machine bolts. Because acoustical measurements are not to be made in the model, the acoustical characteristics of the materials used are of no importance. The wedge size corresponds to a full-scale wedge 8" x 24" x 36" long (0.2m x 0.61m x 0.9m long).

In order to supply the required volume flow for the experiment, the auxiliary fan from the AFRF was obtained; this is part number 9 in Figure 1. The auxiliary fan is a Joy Corporation Series 1000 axial flow fan with a 23.25" (0.59m) inner diameter and 10" (25.4cm) rotor hub. The test duct inner diameter is 9.5" (24cm), so an adapter shell was added between the fan and the test duct. This adapter is a simple sudden expansion and contains a screen to help minimize flow distortion. The fan is placed in a movable housing, as shown in Figure 5, and is coupled to the one-sixth-scale model in such a manner that its exhaust flow paths resemble those anticipated for the full-scale chamber, Figure 10.

2.1.3 Description of the Data Acquisition System

A schematic diagram of the data acquisition system is given in Figure 11.

2.1.3.1 The Probe Rake

The probe rake is shown in Figures 12, 13 and 14. The three five-hole probes mounted on support stems are at radii of 4.15" (10.5cm), 2.75" (7cm), and 1.25" (3.2cm) in a measurement plane which is 4.1" (10.4cm) downstream of the tangent point between the test duct and bellmouth. They are spaced 120 degrees apart. A five-hole probe senses pressure in five principal directions. Four of the five pressure-sensing holes lie in two perpendicular planes with the line of intersection of the two planes passing through the fifth, central hole. The velocity component in any plane in space can be obtained independently from three pressure measurements in the plane

(Pien, 1958). From the five pressure measurements provided by the five-hole probe (obtained in a non-nulling mode), the three orthogonal velocity components at the point of measurement can be derived. Treaster and Yocum (1979) give a complete description of this experimental technique. The probe radii were chosen such that the outermost and innermost probes would be out of the turbulent boundary layer of the test-duct wall and the rake base, respectively. At the measurement plane, the turbulent boundary layer along the duct wall was calculated to be 0.15" (4mm) thick. The outermost probe is 0.6" (15mm) away from the duct wall, well out of the turbulent layer. The turbulent boundary layer along the rake base was tripped by adding a 0.0152" (0.39mm) diameter trip wire 0.4" (10mm) downstream of the nose. At the measuring plane, the turbulent boundary layer along the rake base was calculated to be 0.14" (3.6mm) thick. The shortest probe used is 0.63" (16mm) away from the rake base.

Each five-hole probe was individually calibrated in the laminar core of a free round jet calibration facility. The five-hole probe tip diameter is 0.0625" (1.6mm), and the probe support is six probe diameters downstream of the probe tip. All of the pressure tubes leading to the five-hole probes are taped and fastened to prevent them from fluttering. The five-hole probe pressure measurements are performed at a discrete number of circumferential steps. A 4 second time delay is implemented between each step to allow possible pressure surges in the line to settle out. The five-hole probes are insensitive to fluctuating pressure of frequency greater than about

1 Hz. Hot-wire anemometry is used to measure fluctuating velocities. The hot-wire probe is mounted such that its wire is 2" (5.1cm) behind the measurement plane of the five-hole probes, at a radius of 2.55" (6.5cm). The hot-wire probe was calibrated three different times during the course of the experiment, and its sensitivity was found to drift slightly. Microscopic inspection of the probe revealed that this drift was due to a build up of foam particulate from the wedges. The total drift over the duration of the experiment was less than 1%. Mean voltages were measured with an integrating voltmeter having a 10 second time constant. The fluctuating voltages were measured simultaneously using an rms voltmeter having a 30 second time constant.

As a reference velocity indicator, a pitot-static tube is mounted through the duct wall between 11 and 12 o'clock looking downstream; as shown in Figure 12.

2.1.3.2 The Electronic Equipment

Photographs and an identification of the electronic equipment used are given in Appendix A. All of the electronic equipment was calibrated at the start of the experiment. A calibration check midway through the testing revealed no equipment drift.

2.1.4 Experimental Procedure

The experimental procedure is discussed in two parts: data acquisition and data reduction. Data acquisition is performed manually and by the Digital Controller/Data Acquisition System (DC/DAS) designed and assembled at the Applied Research Laboratory.

Data reduction is accomplished using a Digital Equipment Corporation VAX 11/782 computer, with five-hole probe data reduction software written at the Applied Research Laboratory.

2.1.4.1 Data Acquisition

The probe rake must be manually stepped to its starting position; this is with the longest radius five-hole probe positioned at 12 o'clock. After installing the test inlet wall and sealing the chamber, the auxiliary fan is started and brought up to speed. The DC/DAS is initialized and started, and automated data acquisition begins. The DC/DAS steps the scanivalve pressure-line multiplexer to the position corresponding with the first five-hole probe pressure line. The DC/DAS pauses for 4 seconds, allowing possible pressure surges in the line to settle out, then reads the voltage at the pressure transducer and records it on paper tape. The scanivalve multiplexer is stepped to read the pressure at the next five-hole probe pressure line, and the procedure is repeated until all 15 of the five-hole probe pressure lines' corresponding voltages have been recorded. The scanivalve is then stepped to the 2 pitot-static probe pressure lines, and their corresponding voltages are recorded as above. The last measurement recorded on paper tape for each probe-rake position is the temperature in the vicinity of the probes; it, too, is recorded as a voltage.

While the DC/DAS is automatically acquiring the above data, hot-wire anemometer data are recorded manually. For each probe-rake position the hot-wire anemometer's output voltage is measured by an integrating voltmeter with a 10-second time constant, and

simultaneously by an rms voltmeter with a 30-second time constant. These two voltages and the temperature at the corresponding time of measurement, are recorded manually. The hot-wire anemometer's output voltage is also recorded on an X-Y plotter for 30 seconds in the first probe-rake position.

After the DC/DAS has completed data acquisition for a given probe-rake position, the DC/DAS automatically prompts the stepping motor controller, and the stepping motor rotates the probe rake to the next position.

There are 41 probe-rake measurement positions, each 9° apart; the first and last probe-rake positions are the same. The DC/DAS must be interrupted after the 41st position to stop the data acquisition process.

Because the model chamber is a closed-loop system, the circulating air is heated by the fan motor and fluid friction with each pass-by. To keep the model chamber temperature within the temperature bounds which would be expected in a full-scale chamber, data acquisition would temporarily be terminated while the chamber doors were opened to allow air exchange with the ambient room air. The chamber would then be resealed, and data acquisition would continue.

2.1.4.2 Data Reduction

The paper tape from the DC/DAS, and the manually recorded hot-wire data are reduced independently of each other. The paper tape is read onto the VAX 11/782 disk and is reduced using software written at the Applied Research Laboratory's Garfield Thomas Water

Tunnel. This software follows Treaster and Yocum (1979), and reduces five-hole probe data. Calibration data for each of the five-hole probes used were recorded with the DC/DAS prior to running the inlet wall tests, and these data are stored in a database which is accessed by the five-hole probe data reduction software. Calibration constants for the pressure transducer and the digital thermometer are also stored in this database. The software produces, for each probe position, a plot of the axial, radial, and tangential velocity components; a printout containing the numerical values of the reduced data, including temperature, probe-tip Reynolds number, and velocity data; and a radial plot of the resultant velocity component in the plane of the test fan rotor. These velocity vectors are calculated by vector summation of the radial and tangential velocity components.

The hot-wire anemometer data are reduced to obtain the axial component of turbulence intensity for each hot-wire probe position. The hot-wire data reduction software accesses a database containing the hot-wire calibration data; the hot wire is calibrated with velocity and temperature as variables. For each of the measured temperatures, rms voltages (e'), and mean voltages ($\bar{e}$), the axial turbulence intensity is calculated as (DISA type 55D01 anemometer unit instruction manual):

$$\text{Percent Turbulence Intensity} = \frac{(4)(e')(\bar{e})}{(B)(U)^{1/2}} \times 100 \quad ,$$

where U is the calibration velocity corresponding to $\bar{e}$ and the measured temperature, and B is the slope of the calibration curve plotted as $(\bar{e})^2$ on the ordinate, and $(U)^{1/2}$ on the abscissa, for the measured temperature. The resulting turbulence intensity is plotted for each hot-wire probe position.

CHAPTER III

EXPERIMENTAL RESULTS

3.1 Description of the Inlet Walls and Discussion of the Steady-State Results

A total of five inlet configurations are reported. To maintain as much of a working volume as possible inside the chamber, these inlet walls were designed for the back wall only. Side wall inlets would have required a larger plenum between the two rooms to allow ductwork placement, and would have thereby reduced the size of the inner room.

As a test of the data acquisition system, an ideal flow field was set up through removal of the bellmouth and installation of a 4" (10.2cm) thick honeycomb flow straightener in its place at the end of the test duct. The measured velocity was purely axial, demonstrating that both the probe rake and the flow straightener were performing properly.

A reference cofiguration is required so that improvements due to the inlet walls can be evaluated. The ideal reference configuration would have the inlet duct in a free-space environment; that is, with no walls or boundaries nearby. This is an unrealizable configuration. The next most desirable configuration would have the inlet duct bounded on one side only, for example, by the ground. Finding a space large enough for this configuration is difficult, particularly because outdoor sites are subject to atmospheric disturbances. Not being able to use either of these free-space configurations led to the use of the scale-model anechoic facility, with no test inlet wall, as the

reference configuration. This reference configuration takes account of any model asymmetries and irregularities. (The model is constructed of lumber and steel, and is, accordingly, limited in its accuracy. Likewise, the fan and inlet duct were aligned as accurately as possible, but, due to their large scale and weight, may be slightly misaligned.) The reference configuration is called the open-back case because there is no inlet wall in place, as shown in Figure 15. The open-back case cannot be considered as a practical full-scale chamber configuration because its anechoic, flow straightening, and turbulence properties are poor.

Results from measurements made in the open-back configuration are shown in Figures 16 and 17. These data are obtained from the five-hole probe measurements. V_∞ is the reference axial velocity as measured by the pitot-static probe. The arrows in the radial plot, Figure 16, represent the velocity vectors in the plane of the test fan rotor, which are obtained by the vector summation of the radial and tangential velocities at each measurement point. The length of each arrow indicates the magnitude, and the arrow point indicates the direction, of the resultant velocity vector in the plane of the test fan rotor. For each probe, the 360° spatial mean is subtracted out, leaving only the magnitude of the variation from the spatial mean as the length of the arrow. This view is taken looking downstream into the probe rake; that is, towards the fan unit from the anechoic chamber. Ideally, the flow entering the duct will be irrotational, and the direction of the flow in the duct would be purely axial.

This radial plot would then be made up only of dots, one at each measurement position, indicating that there is no steady-state flow in either the radial or tangential directions.

Figure 17 is a plot of the normalized axial velocity at each of three radii. The velocity at each radius is normalized to V_{∞}, the reference velocity measured with the fixed position pitot-static probe. Zero degrees is at 12 o'clock, and the degree increments proceed in the clockwise direction around the duct looking downstream. Ideally, there would be no variations in the axial flow velocity throughout the cross section of the measuring plane. Such an ideal case would be plotted as three straight lines, each of unity value.

The results for the open back configuration indicate two strong counter-rotating vortices in the plane of the test fan rotor, and a small amount of axial non-uniformity.

Test wall number three is shown in place in Figure 18. At the time of the photo, the width of the vertical slots had been increased by 1.1" (2.79cm) in preparation for assembling test wall number four; other than this change, the wall in the photo is identical to test wall number three. The total open inlet area, 2.5 ft^2 (0.232m^2), was calculated so that the velocity through the wall would be 3.33 fps (1.016 m/s) at a full-scale flow of 300 cfs (8.5 m^3/s). The slots are 1.25" (0.032m) wide and total 290" (7.37m) in length. The inside of the wall is lined with wedges as shown in Figure 19. They are mounted so as to act as flow straighteners and linear diffusers for the incoming air. From an acoustical standpoint, this wall is better than an open back chamber in that 89% of the chamber's back wall is

covered with wedges. From an aerodynamic standpoint, incoming air will experience a sudden contraction as it enters the inlet wall. The absorptive wedges act as linear diffusers to the flow that leaves the inlet wall. This feature would be expected to incite less turbulece than would a sharply edged inlet. The wedges will also act as flow straighteners, aiding in the reduction of large-scale vorticity.

The results for test wall number three are shown in Figures 20 and 21, and a substantial improvement toward the desired pure axial case is seen when these results are compared with the open-back case of Figures 16 and 17.

The results from test wall number three indicate that significant improvement of the flow field at the test plane is indeed possible, and that the large-scale vortices seen in the open-back case can be minimized by proper inlet wall design. Two improvements to wall number three brought about the design of wall number four. A ducting configuration was designed which would simultaneously increase the wedge coverage of the back wall to almost 100%, reduce the sudden contraction at the upstream side of the inlet wall, and act as a flow straightener; it is shown in Figure 22. The width of the vertical slots of wall number three was increased by 88%. This increase in area was then occupied by wedges mounted on standoffs on the upstream side of the inlet wall. These rear mounted wedges act as flow straighteners and turning vanes to the entering air, and as absorptive wedges to sound sources located inside of the chamber. Wall number four is shown in Figures 23 and 24. The

steady-state aerodynamic results for wall number four are shown in Figures 25 and 26. Vortices are still visible in the measuring plane, and, in an attempt to reduce these vortices still further, wall number five was designed.

Wall number five is shown in Figures 27 and 28. The slot width was maintained at 2.35" (6cm), as in wall number four, but two additional horizontal cross panels were added to the design. They were added so as to aid in the straightening of the flow which is presumably angled from the top side. This has the same effect as the vertical cross panels which presumably straighten the flow entering from the sides. The total open area remains unchanged at 2.5 ft^2 (0.232m^2) for this configuration. The most significant effect of this alteration can be seen in Figure 29, where the vortices in the test plane are almost completely removed. The disturbance at 0° is due to the coalescence of residual vortices. Figure 30 shows the steady-state axial velocity for this case. Test wall number five has the ability to straighten air passing through it, while at the same time maintaining a low turbulence intensity (this will be discussed further in Section 3.2). It also provides an anechoic chamber wall with very good anechoic design properties. The head loss across the inlet wall is expected to be low because the slots are not filled with any fibrous absorbent for acoustical purposes, nor has a porous wedge design been used to increase the duct area. Adding additional horizontal cross panels appears to be unnecessary.

In an attempt to locate the source of the remaining vorticity near 0°, and to more fully examine wall number five's ability, several other tests were undertaken. The purpose of the first of these was to demonstrate that neither the bellmouth nor the wedge geometry were responsible for the formation of the residual vortices. For this test, the return path from the fan exhaust to the inlet wall was significantly altered. Styrofoam blocks were installed above and below the inner chamber, thereby preventing return flow along the ceiling and the floor, as shown in the photograph of Figure 31. This figure, along with Figure 32, shows the results of this room configuration with wall number five in place. The flow in the measurement plane has changed considerably, demonstrating that the effectiveness of wall number five is dependent upon the quality of the flow which supplies it.

This gives rise to a concern on the design of the entire chamber. For example, the amount of return air flow which can be supplied along the floor of the outer room is dependent upon how the inner room is vibration mounted. In the most extreme case, the inner chamber might rest directly on the floor of the outer chamber, and there will be no return of air along the floor. To investigate this condition, the styrofoam top blockage was removed, and the bottom blockage was left in place. The results are shown in Figures 33 through 36 for the blocked bottom with and without wall number five in place. The results are encouraging in that they are much better than the totally blocked top and bottom case, and that wall number five does have a beneficial effect on straightening the flow. In another trial, a

symmetric flow situation was forced by unblocking the bottom opening and partially blocking the top opening so that the top and bottom openings were of equal area. The results for the open-back configuration with equal top and bottom areas are shown in Figures 37 and 38. The variation in flow field from the case of a totally blocked bottom is small, which is encouraging in that small geometry changes don't significantly alter the flow quality at the measurement plane. Turbulence intensity data for these cases are presented in Section 3.2. Further study of the room configuration, as opposed to the inlet wall configuration, would have required major modification of the experimental set-up and was seen to be well out of the scope of this project. In Chapter IV, a return-flow control system is described which would hopefully alleviate problems of room configuration.

A low velocity test was performed to help in assessing wall number five's capability at speeds other than the maximum test velocity. Figures 39 and 40 show the results for V_∞ = 54 fps (16.46 m/s), approximately one-half of the maximum test velocity. The resulting flow field at the measurement plane is almost identical to the result obtained at full velocity. No turbulence intensity data are available for this case because the hot-wire was not calibrated at velocities below 60 fps (18.29 m/s).

The steady-state axial velocities showed no measurable change from case to case. The very small variations in the steady-state axial velocities appear to be repeatable and unrelated to the other components of velocity.

3.2 Unsteady Flow Results

The axial turbulence intensities for the configurations in Section 3.1 are shown in Figures 41 through 43. Figure 41 contains the results for the open-back case and wall number three, four, and five. As the wall designs are improved from the open-back case through wall number five, there is a general reduction in the overall axial turbulence intensity. The turbulence intensity is calculated as described in Section 2.1.4.2. The maximum axial turbulence intensity for each configuration occurs where the vortices in the plane of the test fan rotor coalesce.

Figure 42 shows the axial turbulence intensity for wall number five with the top and bottom return-flow paths completely blocked. The turbulence intensity maxima have relocated because the locations of the vortices have changed.

The axial turbulence intensity data in Figure 43 is for the bottom blockage alone and partial top blockage configurations. For the open-back case, the effect of changing the blockage is detectable in the turbulence intensity data. Installing inlet wall number five substantially reduces the turbulence intensity, even for this case of altered return-path flow.

3.3 Repeatability

To demonstrate repeatability, one of the first test runs was repeated. Figures 44 and 45 show the results for a test performed at the start of the final testing phase. Figures 46 and 47 show the results for a test performed after the completion of the final testing

phase. The agreement is good except for the point at -5° at the middle radial position, because this point is in the wake of the pitot-static tube. To again demonstrate the effectiveness of inlet wall number five, it was installed for this case of V_∞ = 90 fps (27.43 m/s). The results are shown in Figures 48 and 49. Turbulence intensity results for these three cases are shown in Figure 50.

CHAPTER IV

SUMMARY, CONCLUSION, AND RECOMMENDATIONS FOR FUTURE RESEARCH

4.1 Summary of Results

Guided by the aerodynamic and acoustical criteria set forth in Chapter I, test walls were successively designed which had an increasingly beneficial effect on straightening the flow and reducing the turbulence intensity in the plane of a hypothetical test rotor mounted in a duct. Although not determined experimentally, the anechoic capability of the best inlet wall would be expected to be unaffected because of its nearly 100% coverage by wedges. The sound transmission loss capabilities of the wall were not considered because auxiliary fan noise could be effectively controlled at a location closer to the source. The performance of the best wall design was found to be limited by the quality of the return air supplying the inlet wall. Small changes in the symmetry of the return air supply appeared to have a negligible effect on the flow field at the measuring plane, while large scale return flow path alterations were capable of inducing vortices and turbulence which were significant in the plane of the test rotor. The best wall's performance was found to be independent of velocity.

The design of the final wall is based on a rear-mounted wedge system which allows an unrestricted flow of air, anechoic behavior, and aerodynamically beneficial performance such as flow straightening and low turbulence generation. It is believed that any attempt to further improve the wall's behavior in one of the above areas would

degrade its behavior in one or more of the others. The characteristic rectangular inlet is based upon rectangular wedges being the conventional anechoic chamber wall covering.

4.2 Conclusion

This experimental study demonstrates that a carefully designed inlet wall can share aerodynamic and acoustical capabilities, and provide an environment for aeroacoustic studies which is superior to outdoor sites and anechoic chambers without flow straightening capabilities.

4.3 Recommendations for the Design of High-Volume-Flow Subsonic Anechoic Chambers for Use in Aeroacoustic Studies

The most basic element of the system described herein is the duct/wedge configuration detailed in Figure 22. This configuration serves three purposes: It maintains the anechoic capability of the inlet wall; it acts as a flow straightener; it acts as a linear contraction, a linear diffuser, and a flow separator. Understanding these three devices aids in the proper design of the duct/wedge unit. For example, the rear mounted wedge must have a base width which is larger than the slot width to prevent acoustical reflections from entering the anechoic chamber, and must be long enough to enter into the chamber and maintain the specified chamber low frequency cutoff. For this reason there must also be an airspace behind the rear mounted wedge. From a flow standpoint, a smooth wedge covering should be chosen as to minimize one mechanism which can lead to premature turbulent boundary layer flow over the wedge.

Placement of the inlet slots is also of importance. If it were possible to structurally support them, small crosses of duct/wedge systems would provide the optimal flow straightening capability. Given that this will often not be an easily achieved goal, long runs of inlet slots in any one direction will provide a good result, but these should be broken up by flow straightening wedges running in the perpendicular direction. Inlet slots should not be less than one wedge length from any side wall; this will lessen the effect of vortices forming at the boundary layer due to the wedges at the sidewall. Although not studied in detail, the rounding off of the sharp corners of the slots may provide additional improvements in turbulence suppression.

The effect of inner room placement and return flow quality is a topic which was not examined in depth in this thesis. Results were presented, though, which show cause for concern in the design of return flow paths. The use of a return-flow control system can serve two purposes: provide a control system whereby the flow which supplies the inlet wall can be varied; and provide a mechanism for attenuating noise from auxiliary air moving equipment before it reaches the inlet wall. A typical system might direct the exhaust of the air moving system to an acoustically damped manifold which exhausts to several silencers. The silencers then connect to duct-work which is treated and sized to aid in acoustic attenuation, and eventually leads to the inlet wedge/duct system. If these ducts are fitted with variable dampers, the return air volume can be varied over different sections of the inlet wall, thereby allowing the

system to be fine-tuned or altered independently of the room structure. The simple addition of a return air control system such as this could prove to be the difference between a successful installation and a poor one.

4.4 Recommendations for Future Research

The most important problem which this thesis has exposed is that of the effect of the quality of the air flow which reaches the inlet wall. Given that, in order to maintain an acoustically and aerodynamically balanced inlet wall, it is impossible for the inlet wall to correct all flow inhomogeneities which it encounters, it would be valuable to study the effect of such features as increasing the plenum space behind the duct/wedge unit, or blocking return paths from the fan exhaust. An interesting follow-on research task would be to actually construct the return-flow control system described in the previous section and investigate the variability and control of the flow field in the desired test region as a function of the return supply.

BIBLIOGRAPHY

Bekofske, K. L.; Sheer, R. E.; and Wang, J. C. F., 1977. Fan inlet disturbances and their effect on static acoustic data. Transactions of the ASME, Journal of Engineering for Power. Paper No. 77-GT-63.

Beranek, L. L., and Sleeper, H. P., 1946. The design and construction of anechoic sound chambers. J. Acous. Soc. America 18(1): 140-150.

Brownell, W. F., 1968. An anechoic flow facility design for the Naval Ship Research and Development Center, Carderock. NSRDC Hydromechanics Laboratory, Research and Development Report 2924.

Bruce, E. P., 1974. The ARL Axial Flow Research Fan - a new facility for investigation of time-dependent turbomachinery flows. ASME Paper No. 74-FE-27.

Cocking, B. J., and Ginder, R. B., 1974. The effect of an inlet flow conditioner on fan distortion tones. AIAA Paper 77-1324.

Duda, J., 1977. Basic design considerations for anechoic chambers. Noise Control Engineering Journal 9(2):60-67.

Gelder, T. F., and Soltis, R. F., 1975. Inlet noise of 0.5 meter diameter NASA QF-1 fan as measured in an unmodified compressor aerodynamic test facility and in an anechoic chamber. NASA TN D-8121.

Hanson, D. B., 1974. Spectrum of rotor noise caused by atmospheric turbulence. J. Acous. Soc. America 56(1):110-126.

Hanson, D. B., 1977. Study of noise and inflow distortion sources in the NASA QF-1B fan using measured blade and vane pressures. NASA CR-2899.

Heidmann, M. F., and Dietrich, D. A., 1976. Simulation of flight-type engine fan noise in the NASA-Lewis 9 × 15 Anechoic Wind Tunnel. NASA TM X-73540.

Ho, P. R.; Smith, E. B.; and Kantola, R. A., 1979. An inflow turbulence reduction structure for scale model fan testing. AIAA Fifth Aeroacoustics Conference, Paper No. 79-0655.

Hodder, B. K., 1973. Investigation of the effect of inlet turbulence length scale on fan discrete tone noise. NASA TM X-62300.

Kantola, R. A., and Warren, R. E., 1979. Reduction of rotor-turbulence interaction noise in static fan noise testing. AIAA Fifth Aeroacoustics Conference, Paper No. 79-0656.

Knudsen, V. O., and Harris, C. M., 1950. Acoustical Designing in Architecture, p. 250. Published by the Acoustical Society of America.

Lowrie, B. W., 1977. The design and calibration of a distortion reducing screen for fan noise testing. AIAA Paper 77-1323.

Peracchio, A. A., 1981. Assessment of inflow control structure effectiveness and design system development. AIAA Seventh Aeroacoustics Conference, Paper AIAA-81-2048.

Pien, P. C., 1958. Five-hole spherical pitot tube. David W. Taylor Model Basin Report 1229.

Povinelli, F. P.; Dittmar, J. H.; and Woodward, R. P., 1972. Effects of installation caused flow distortion on noise from a fan designed for turbofan engines. NASA TN D-7076.

Povinelli, F. P., and Dittmar, J. H., 1972. Installation caused flow distortion and its effect on noise from a fan designed for turbofan engines. NASA TM X-68105.

Preisser, J. S., and Chestnutt, D., 1983. Flight effects on fan noise with static and wind tunnel comparisons. AIAA Eighth Aeroacoustics Conference, Paper AIAA 83-0678.

Rentz, P. E., 1976. Softwall acoustical characteristics and measurement capabilities of the NASA-Lewis 9 × 15 foot low speed wind tunnel. Bolt, Beranek and Newman, Inc., Canoga Park, CA, Rept. BBN-3176; Also NASA CR-135026.

Shaw, L. M.; Woodward, R. P.; Glaser, F. W.; and Dastoli, B. J., 1977. Inlet turbulence and fan noise measured in an anechoic wind tunnel and statically with an inlet flow control device. NASA TM-73723.

Treaster, A. L., and Yocum, A. M., 1979. The calibration and application of five-hole probes. ISA Transactions 18(3):23-34.

Wazyniak, J. A.; Shaw, L. M.; and Essary, J. D., 1977. Characteristics of an anechoic chamber for fan noise testing. NASA TM X-73555.

Woodward, R. P.; Wazyniak, J. A.; Shawn, L. M.; and MacKinnon, M. J., 1977. Effectiveness of an inlet flow control device to simulate flight fan noise in an anechoic chamber. NASA TM-73855.

Yuska, J. A.; Diedrich, J. H.; and Clough, N., 1971. Lewis 9- by 15-foot V/STOL wind tunnel. NASA TM X-2305.

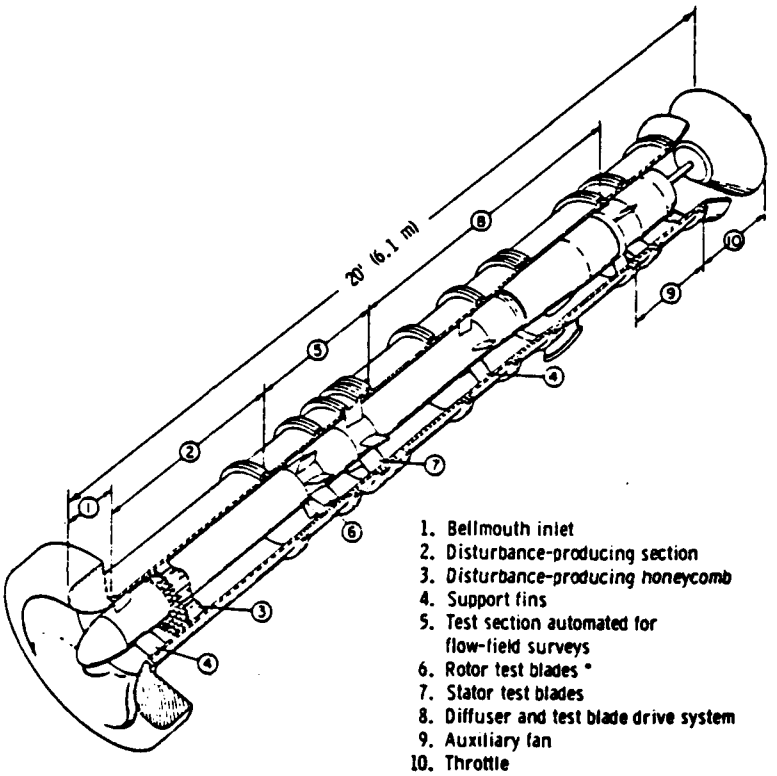

Figure 1. The Applied Research Laboratory Axial Flow Research Fan. From Bruce (1972).

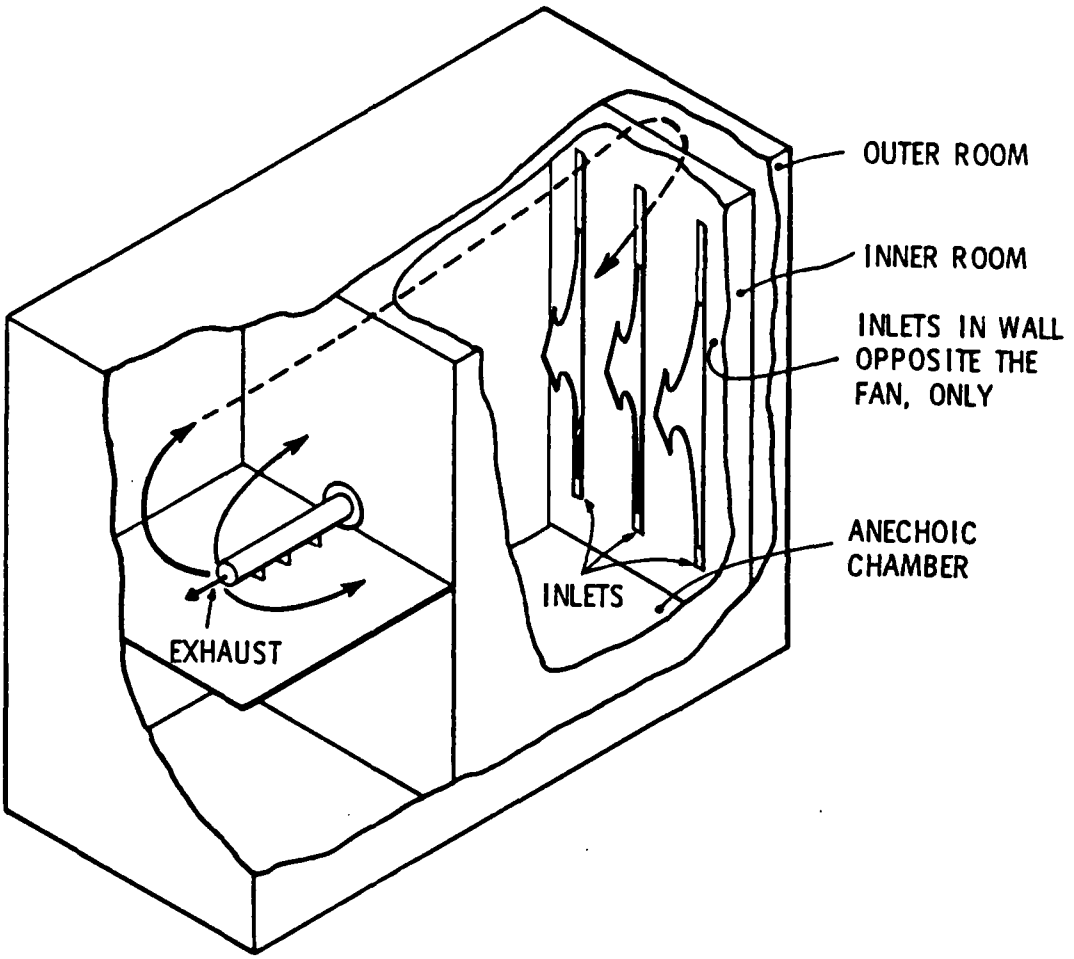

Figure 2. General design concept for the high-volume-flow subsonic anechoic chamber.

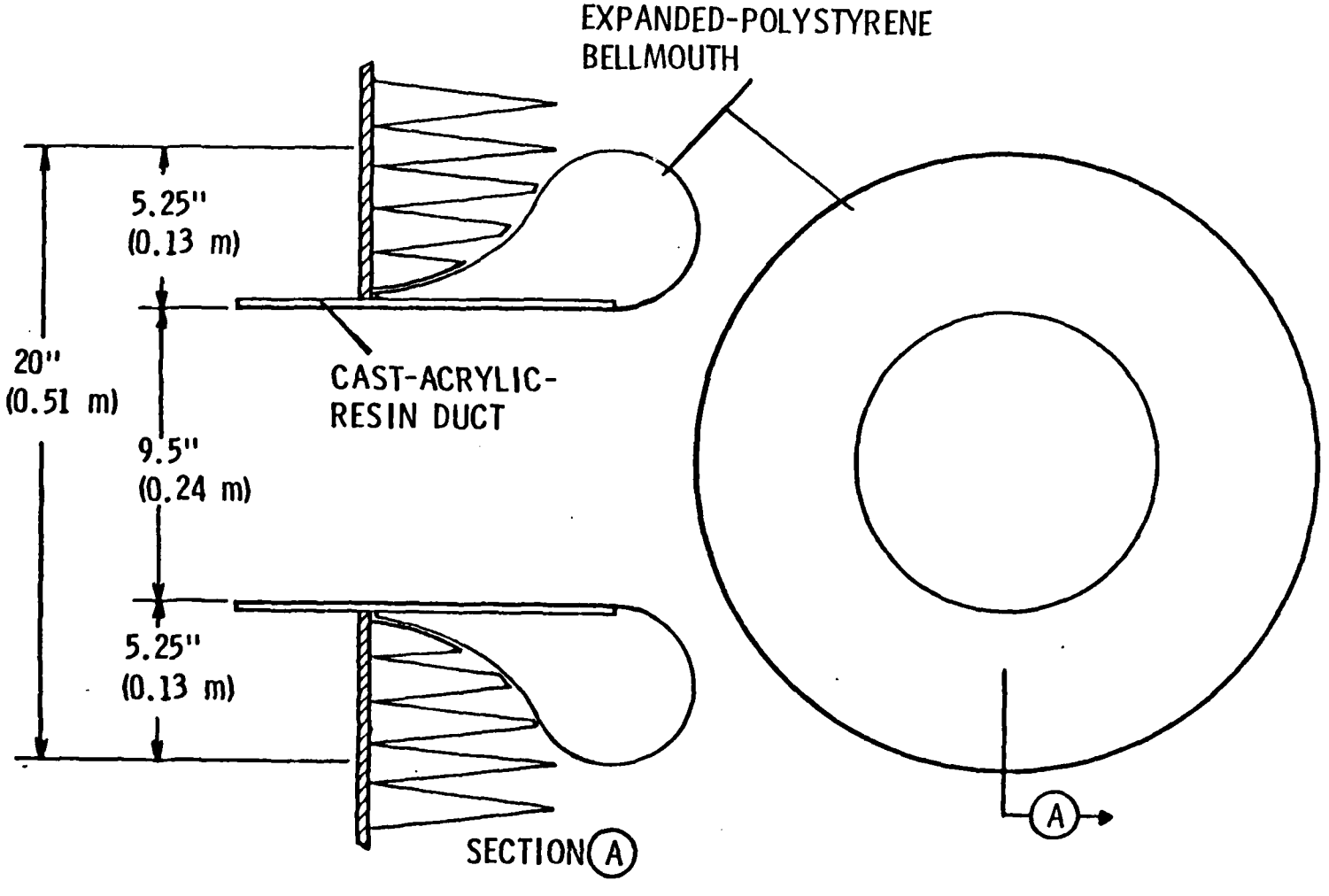

Figure 3. Bellmouth detail.

Figure 4. Exterior view of the one-sixth-scale model.

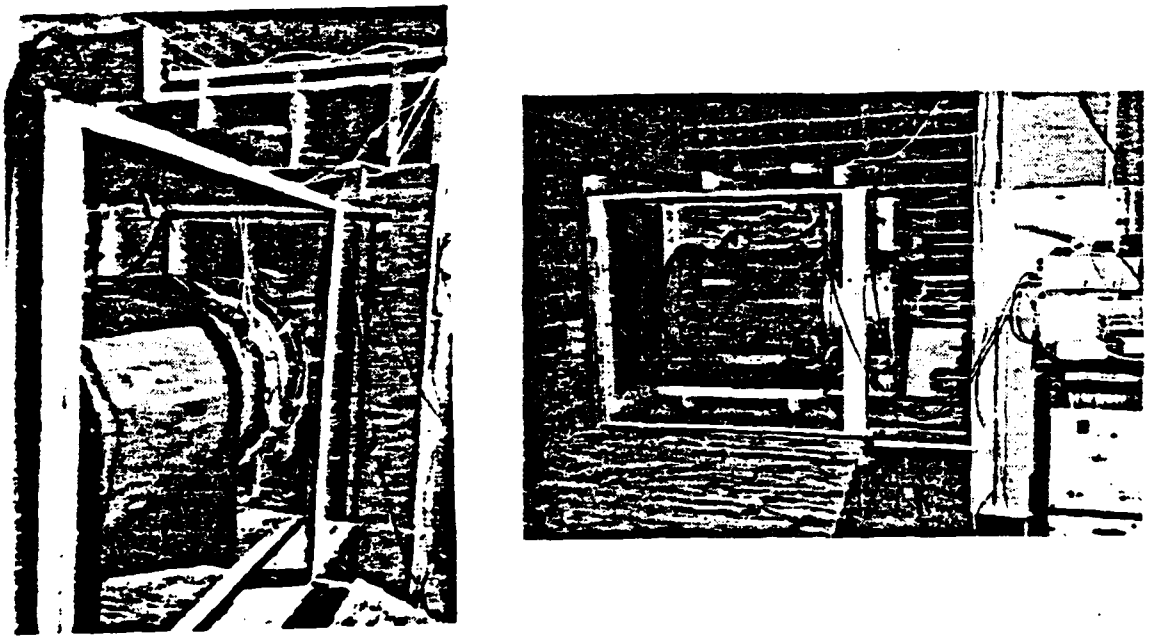

Figure 5. The Joy Axivane fan, shown uncoupled from the one-sixth-scale model, with the fan housing door opened. The 9.5" test duct and stepping motor can be seen in the right hand photo.

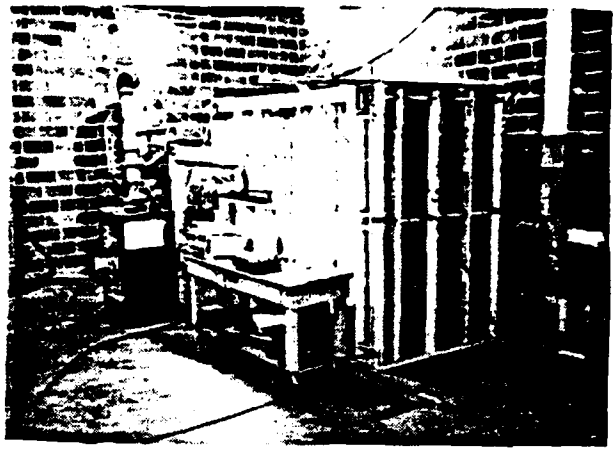

Figure 6. Exterior view of the one-sixth-scale model showing the front door, which allows access to the test chamber.

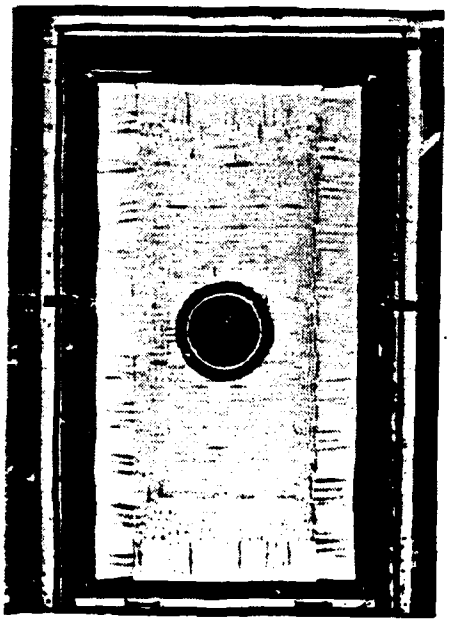

Figure 7. The test chamber as seen with the front door opened and no test inlet wall in place.

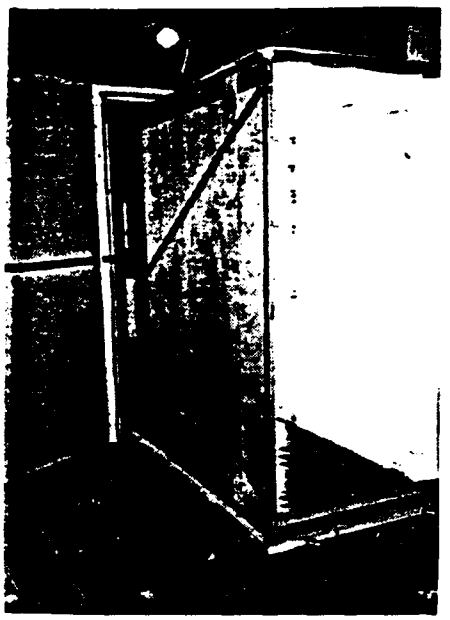

Figure 8. The inner room as seen when rolled out of the outer room.

Figure 9. The outer room, the test duct, and the Joy Axivane fan. The inner room is completely removed.

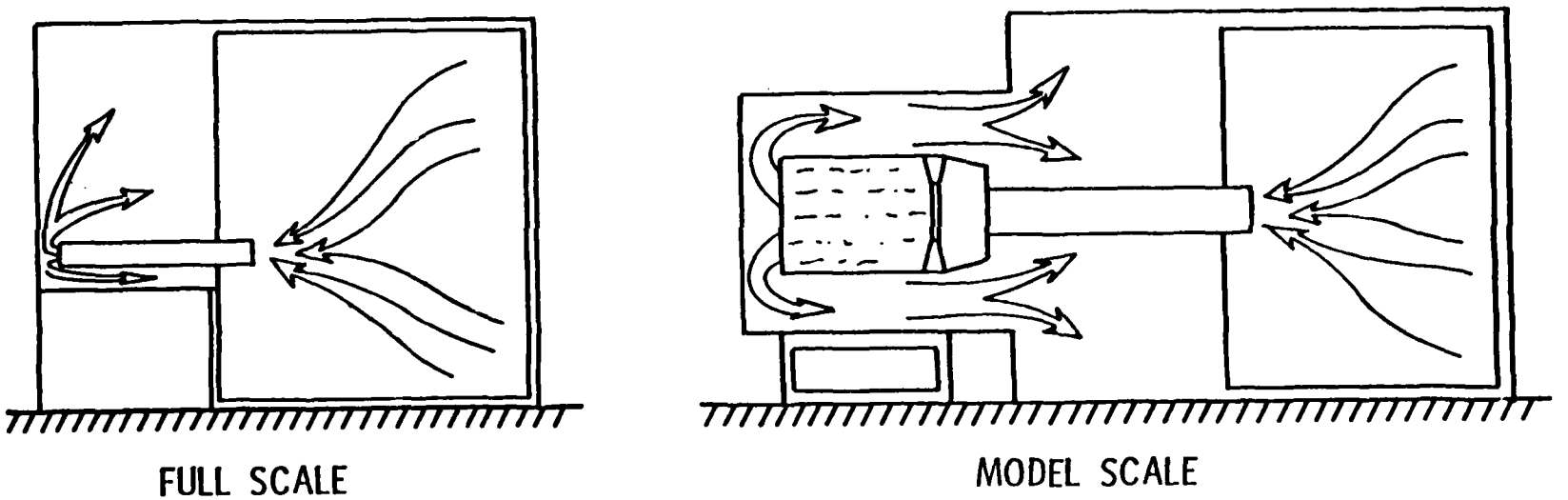

Figure 10. Exhaust comparison.

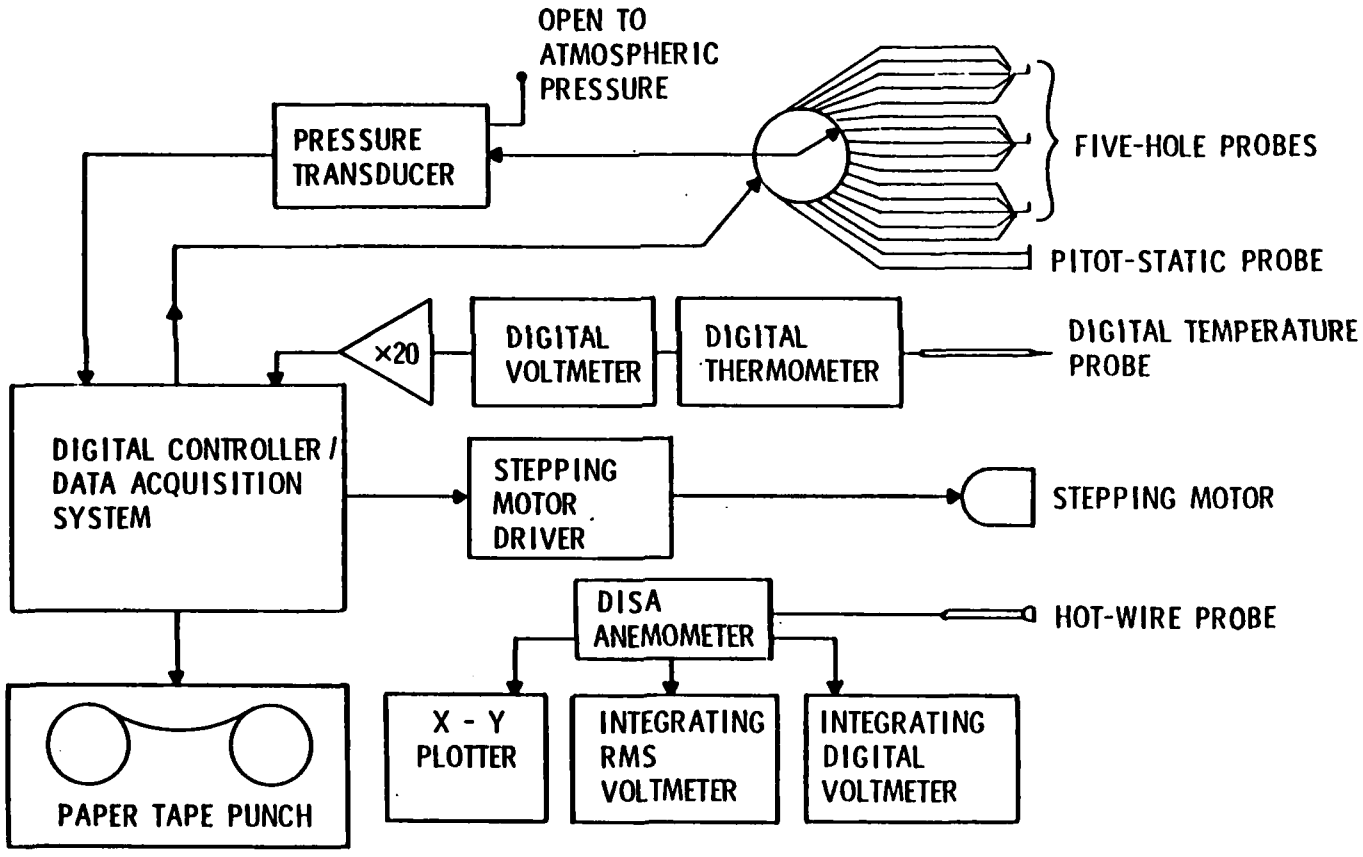

Figure 11. Instrumentation schematic.

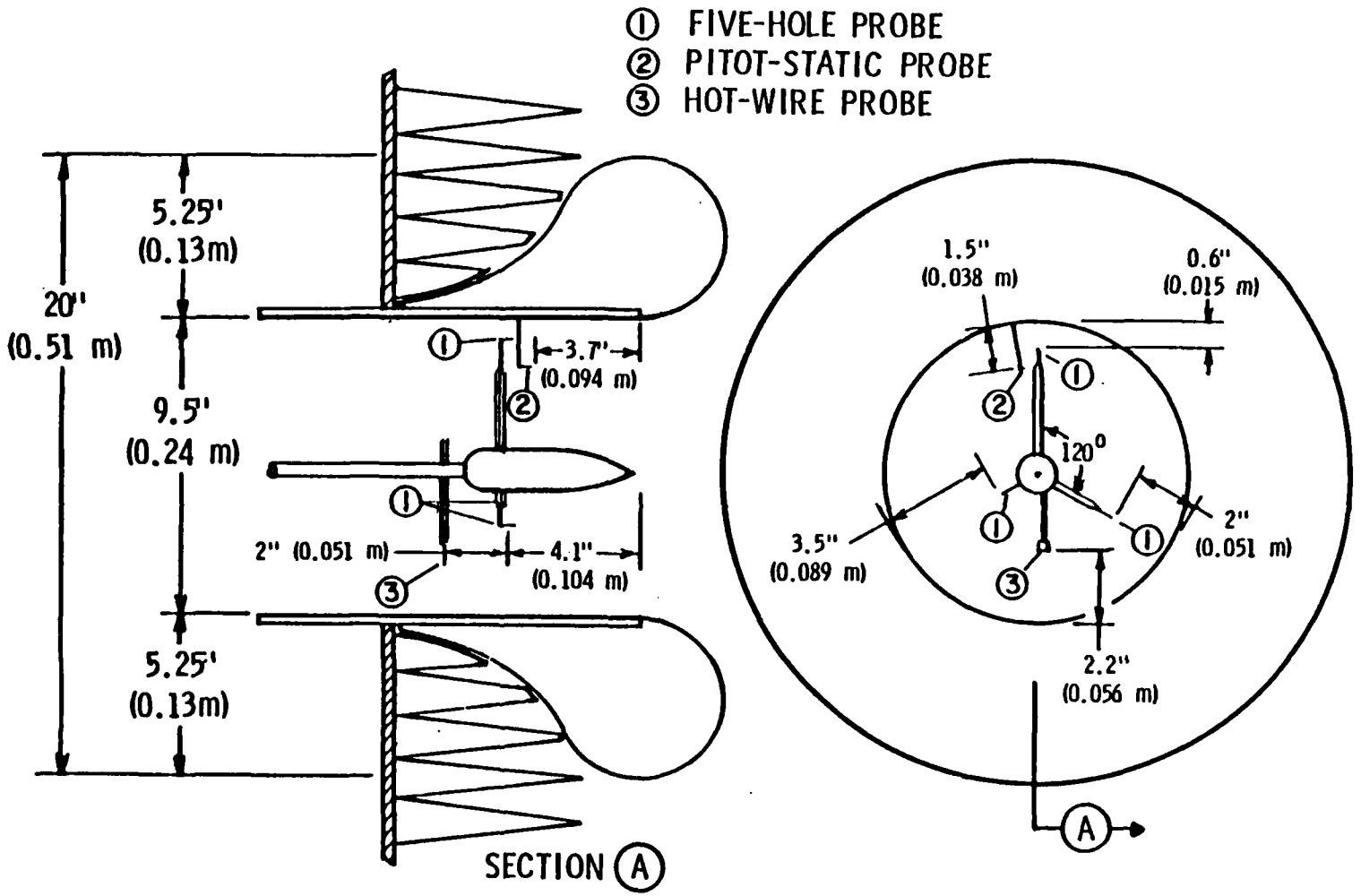

Figure 12. Probe rake detail.

Figure 13. Looking downstream at the bellmouth and the probe rake.

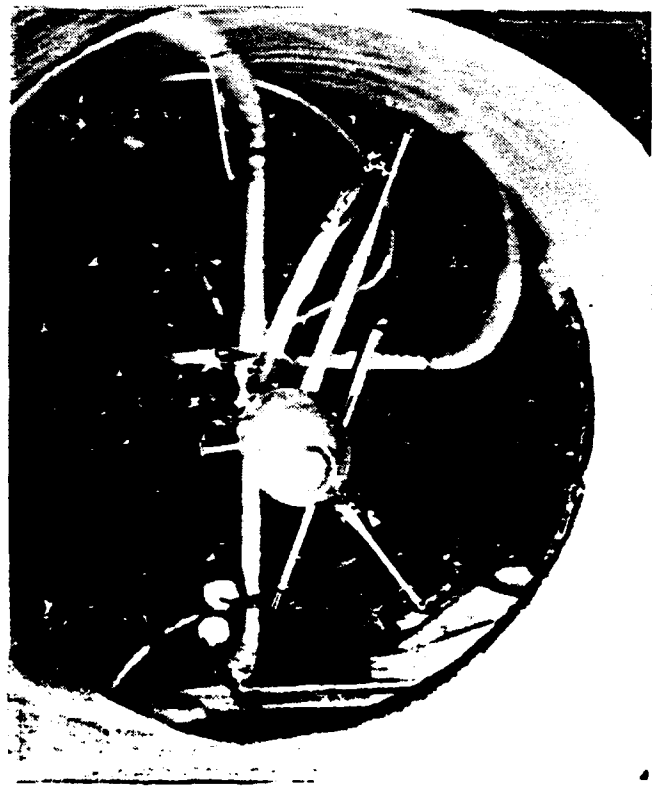

Figure 14. Looking downstream at the probe rake.

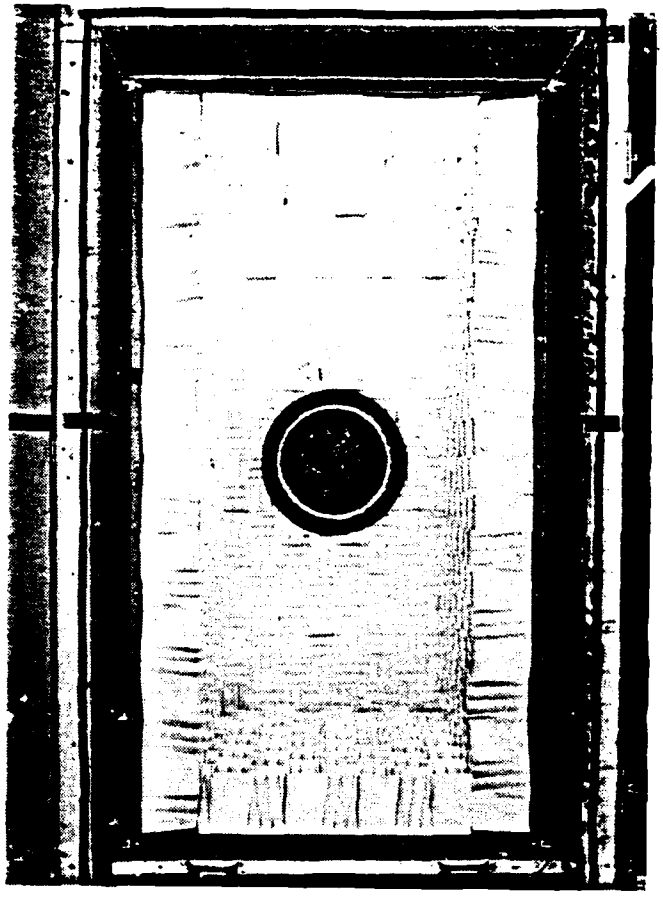

Figure 15. The open-back chamber with no test wall.

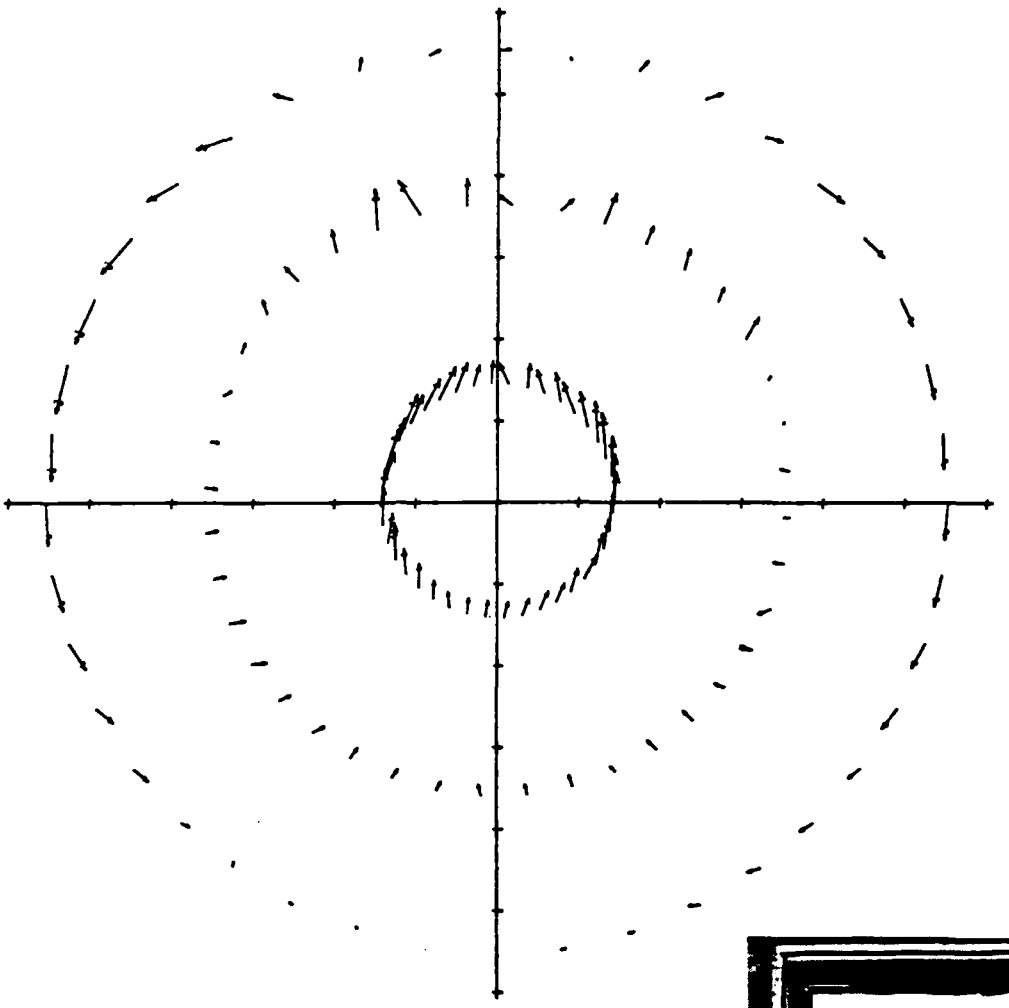

RELATIVE SCALE:
——→ = 0.20V_∞
(MEAN VALUES SUBTRACTED OUT)

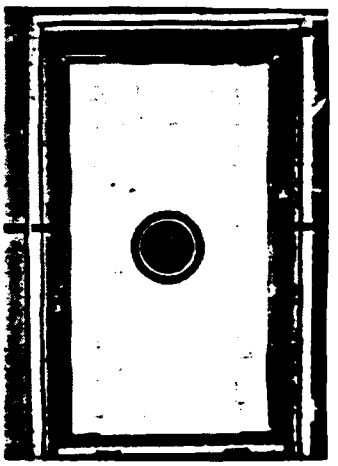

Figure 16. Steady-state flow in the plane of the test rotor, for the case of no test wall. V_∞ = 105 fps (32 m/s).

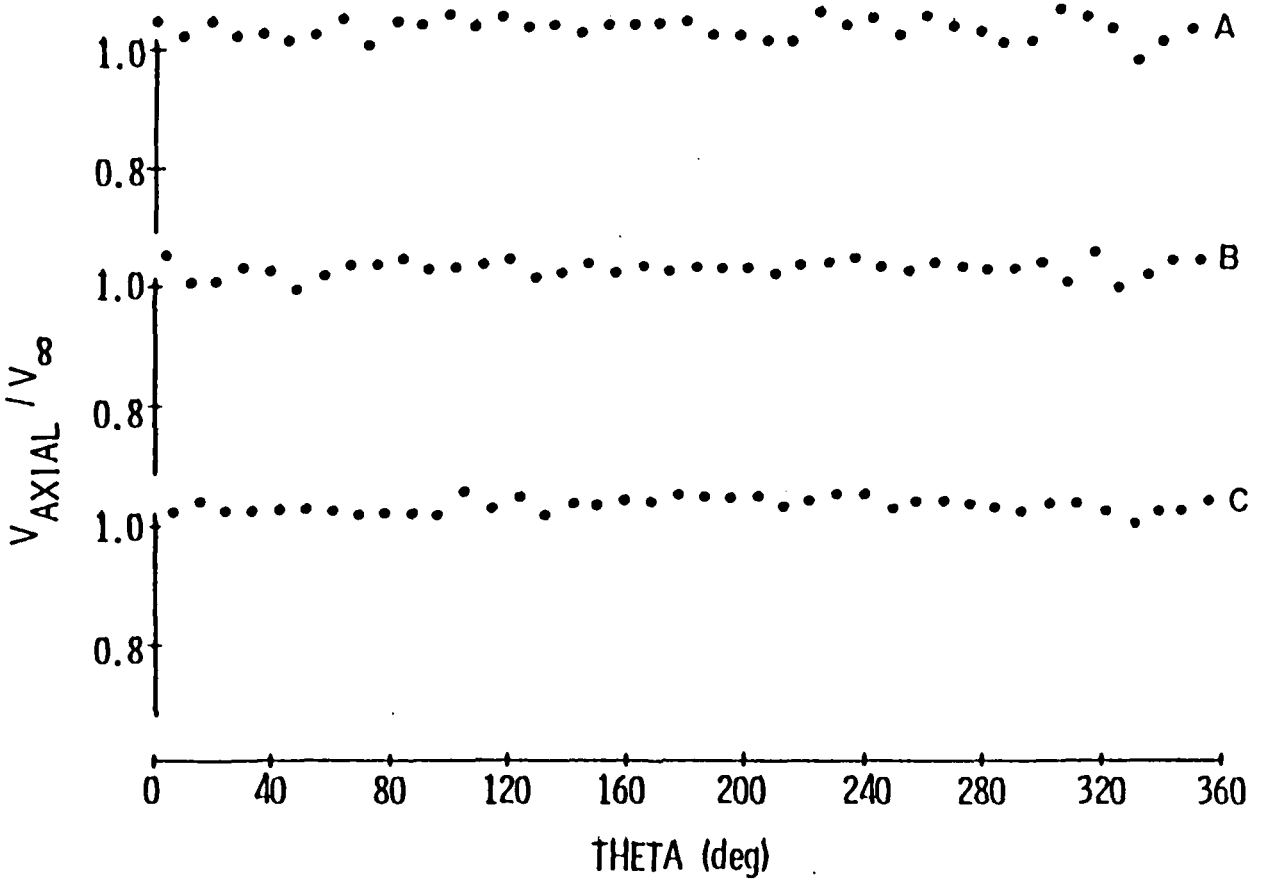

Figure 17. Steady-state axial velocities for the case of no test wall. V_∞ = 105 fps (32 m/s). (A) Radius 4.15" (10.5 cm); (B) radius 2.75" (7 cm); and (C) radius 1.25" (3.2 cm).

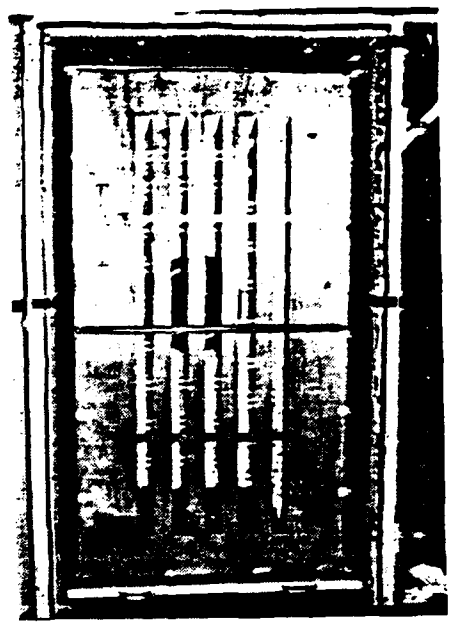

Figure 18. Test wall number three.

Figure 19. Test wall number three as seen from inside the chamber.

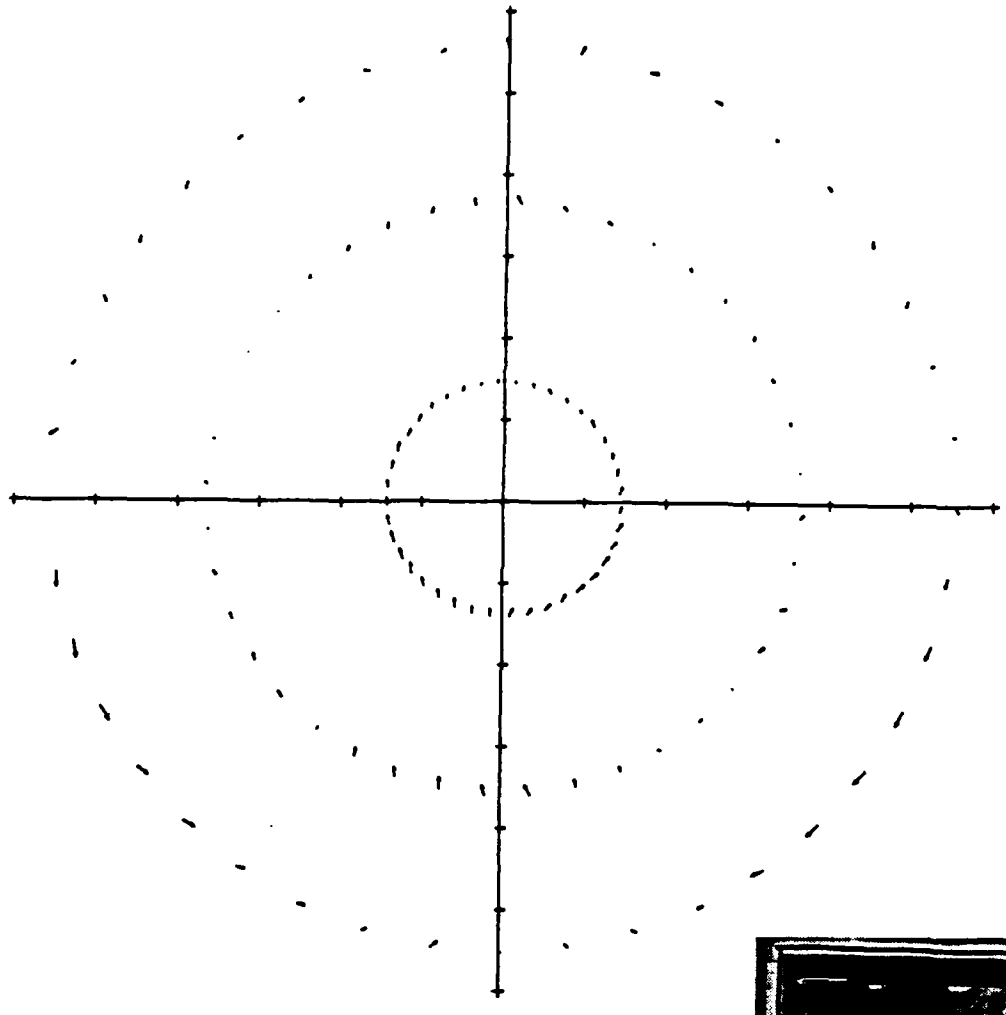

RELATIVE SCALE:
——→ = $0.20V_\infty$
(MEAN VALUES SUBTRACTED OUT)

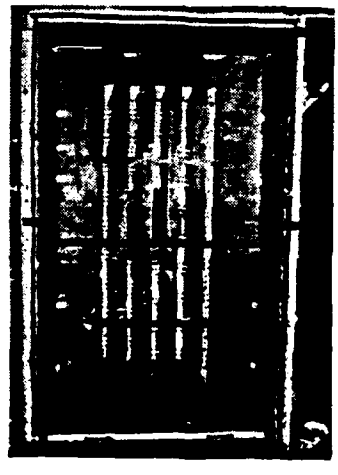

Figure 20. Steady-state flow in the plane of the test rotor, for the case of test wall number three. V_∞ = 105 fps (32 m/s).

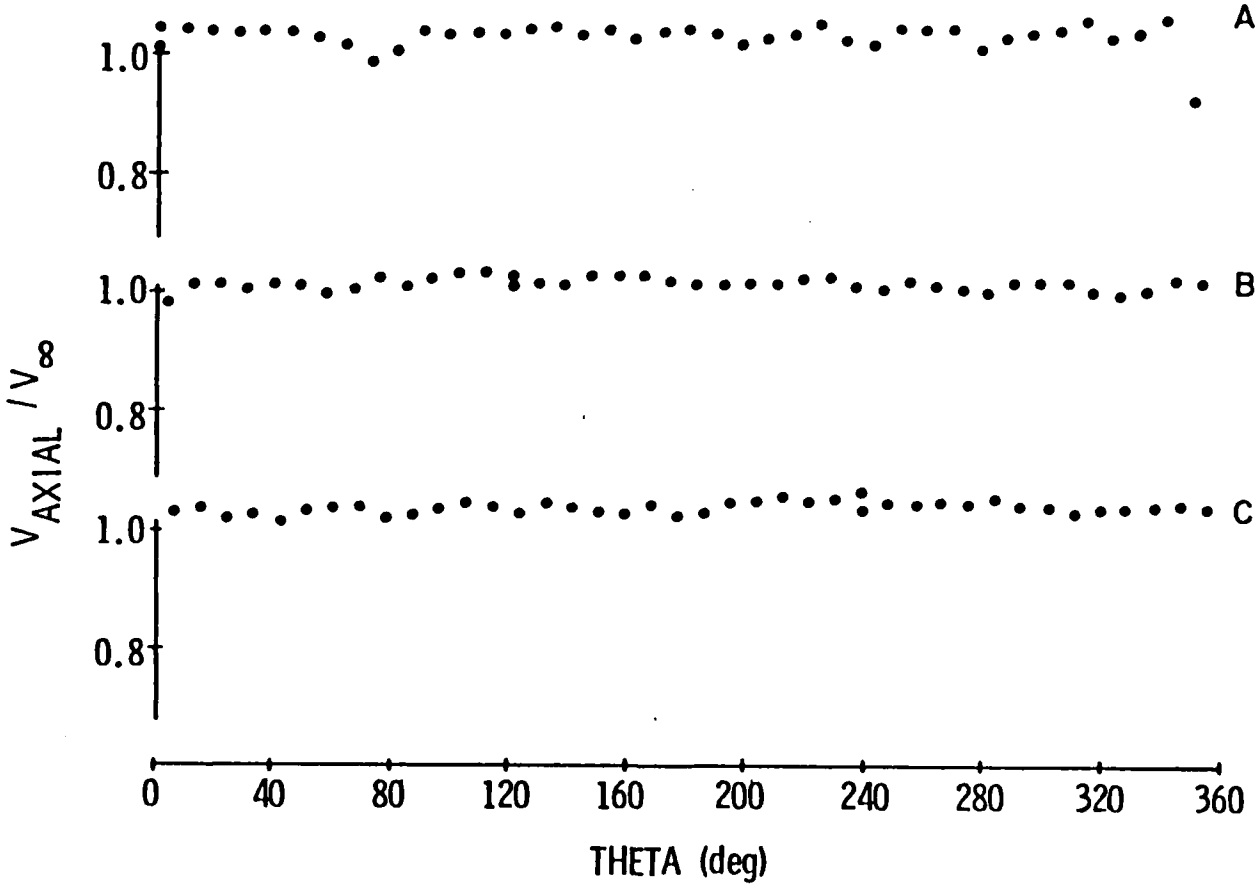

Figure 21. Steady-state axial velocities for the case of test wall number three. V_∞ = 105 fps (32 m/s). (A) Radius 4.15" (10.5 cm); (B) radius 2.75" (7 cm); and (C) radius 1.25" (3.2 cm).

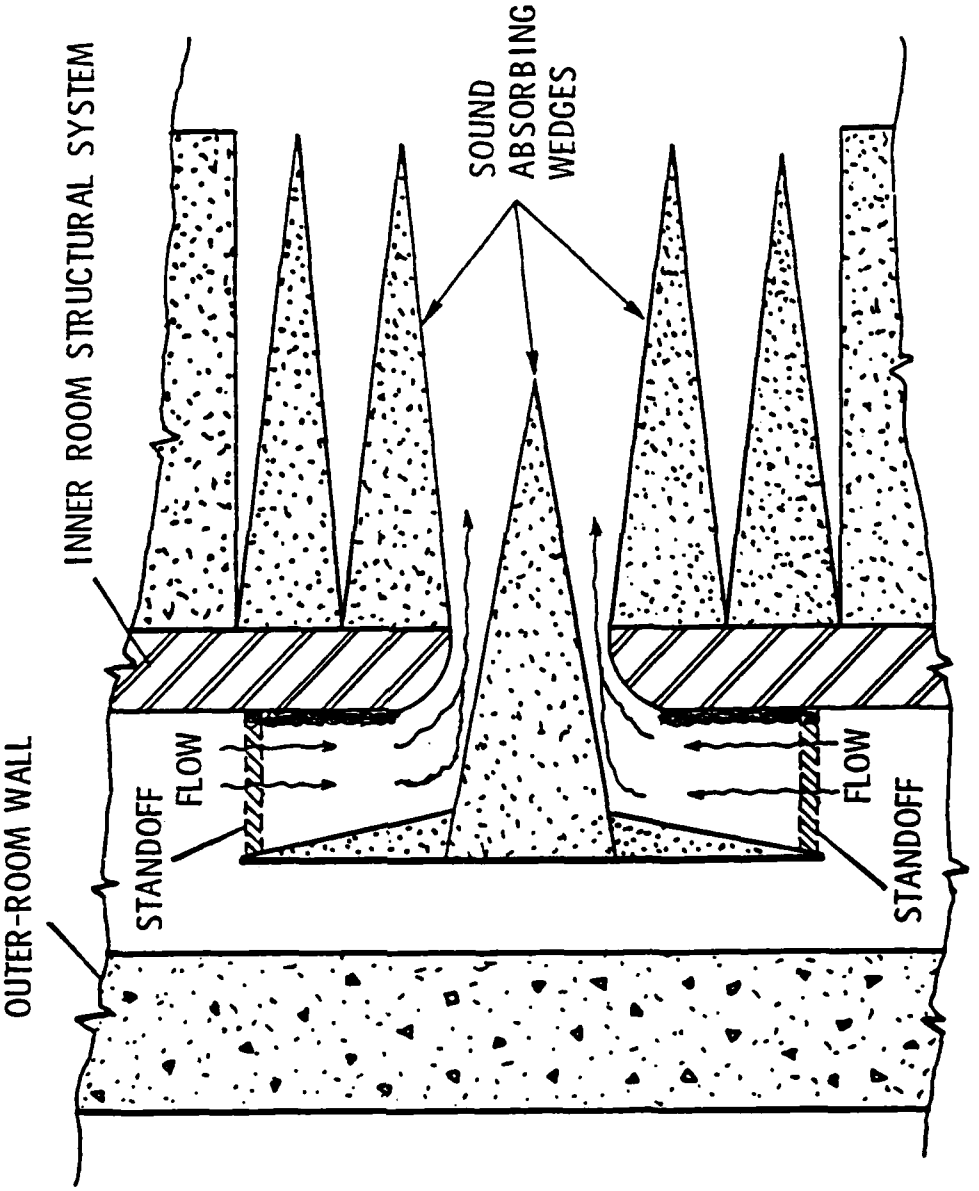

Figure 22. Duct/wedge configuration.

Figure 23. Wall number four shown with the rear-mounted wedges removed.

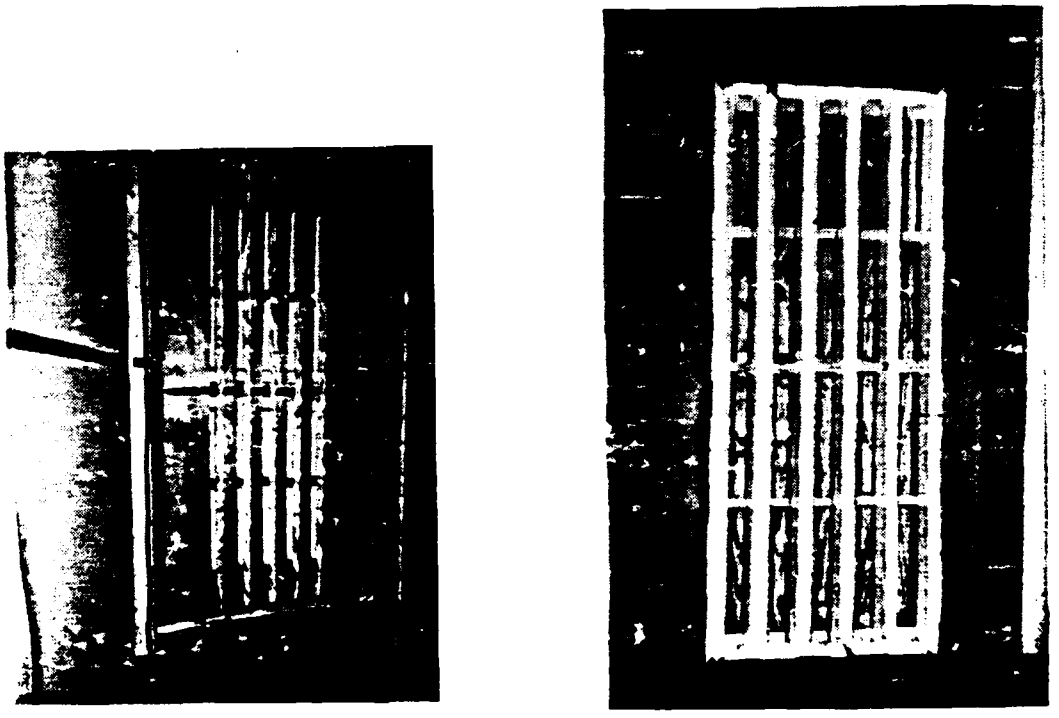

(A) (B)

Figure 24. Wall number four; (A) with the rear-mounted wedges in place; (B) as seen from inside the chamber; the wedges have not yet been mounted on the rear-mounted support strips.

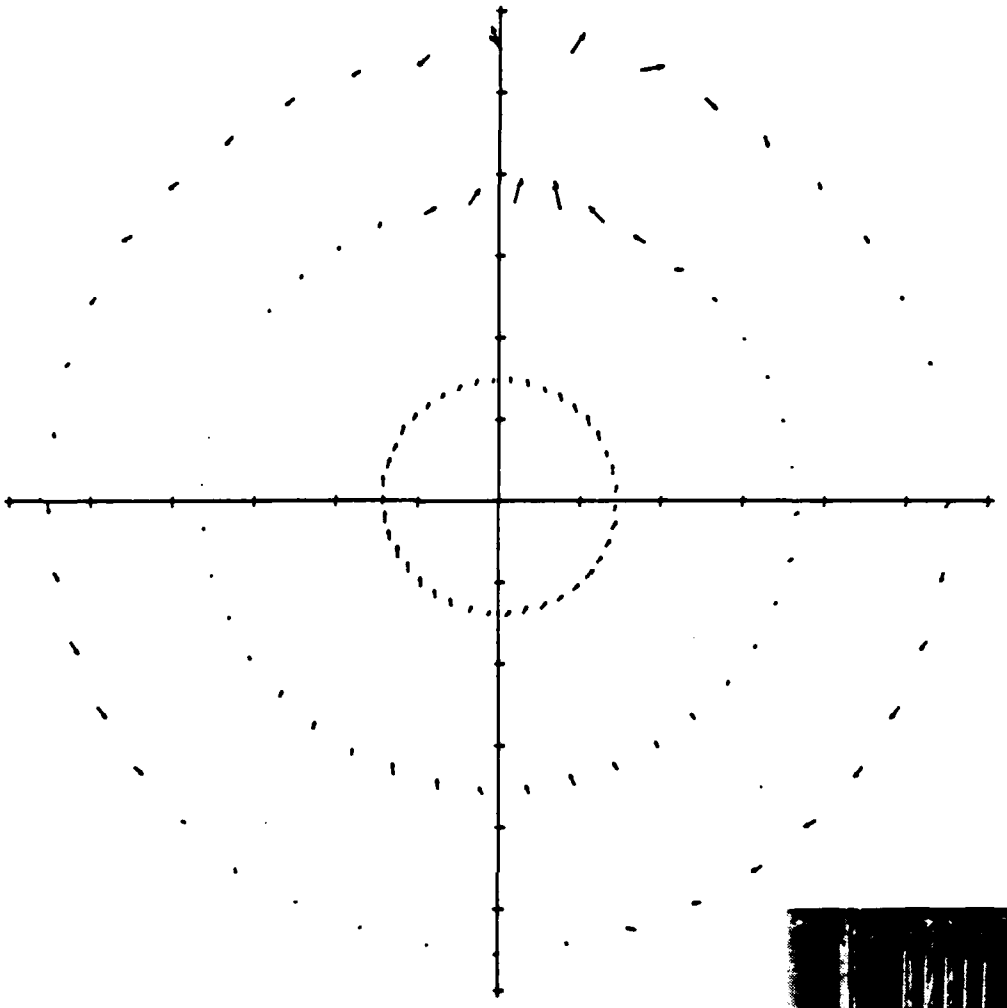

RELATIVE SCALE:
$\longrightarrow = 0.20V_\infty$
(MEAN VALUES SUBTRACTED OUT)

Figure 25. Steady-state flow in the plane of the test rotor, for the case of test wall number four. V_∞ = 98 fps (29.9 m/s).

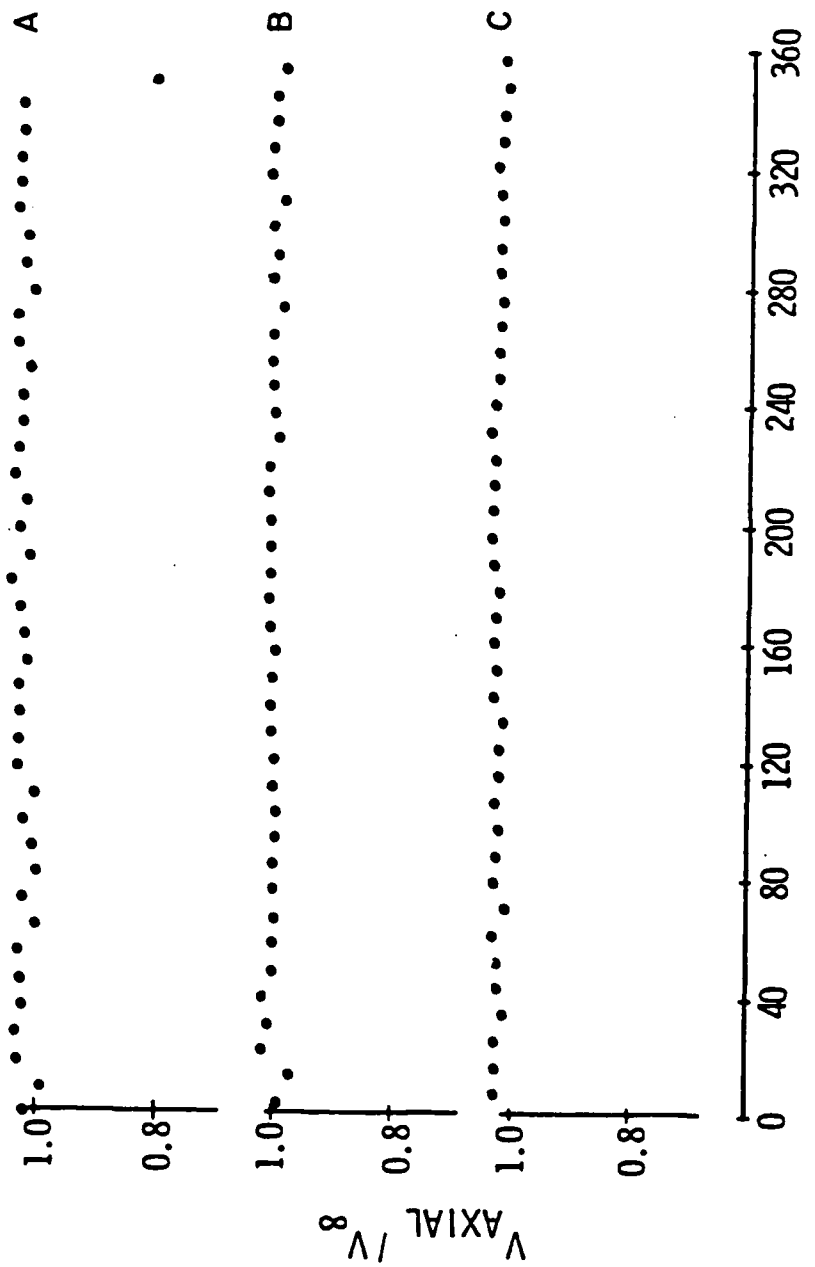

Figure 26. Steady-state axial velocities for the case of test wall number four. V_∞ = 98 fps (29.9 m/s). (A) Radius 4.15" (10.5 cm); (B) radius 2.75" (7 cm); and (C) radius 1.25" (3.2 cm).

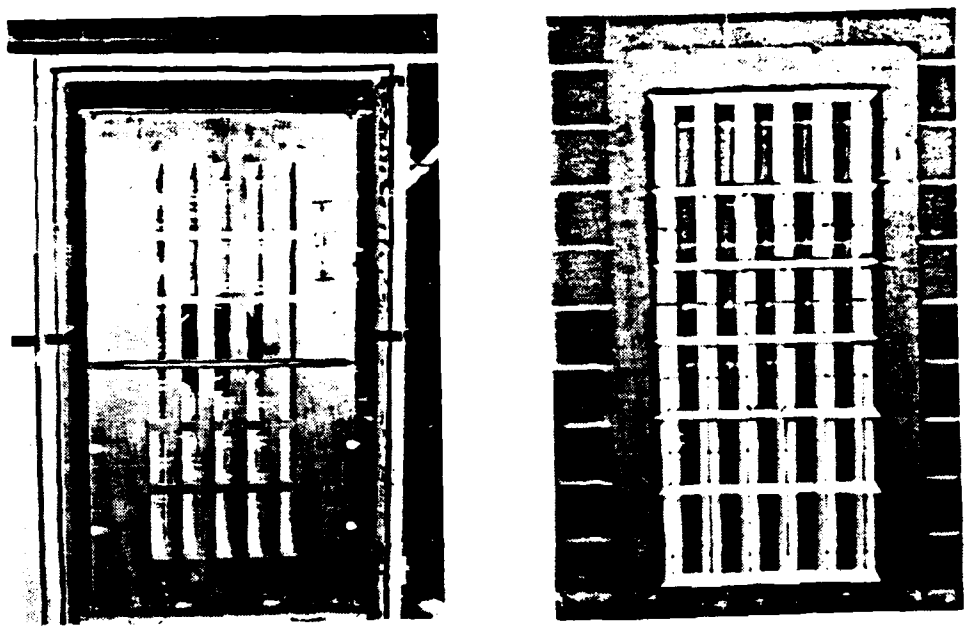

(A) (B)

Figure 27. Wall number five with the rear-mounted wedges removed; (A) as seen from outside of the chamber; (B) as seen from inside the chamber.

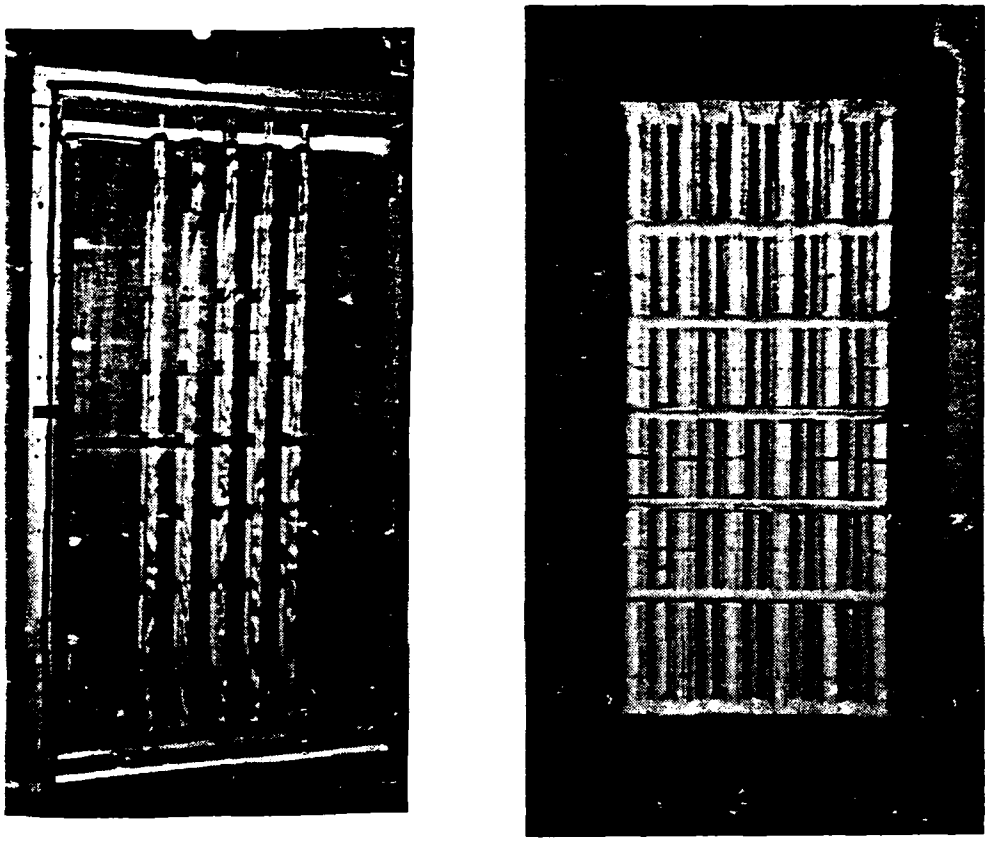

(A) (B)

Figure 28. Wall number five with the rear-mounted wedges in place; (A) as seen from outside of the chamber; (B) as seen from inside the chamber.

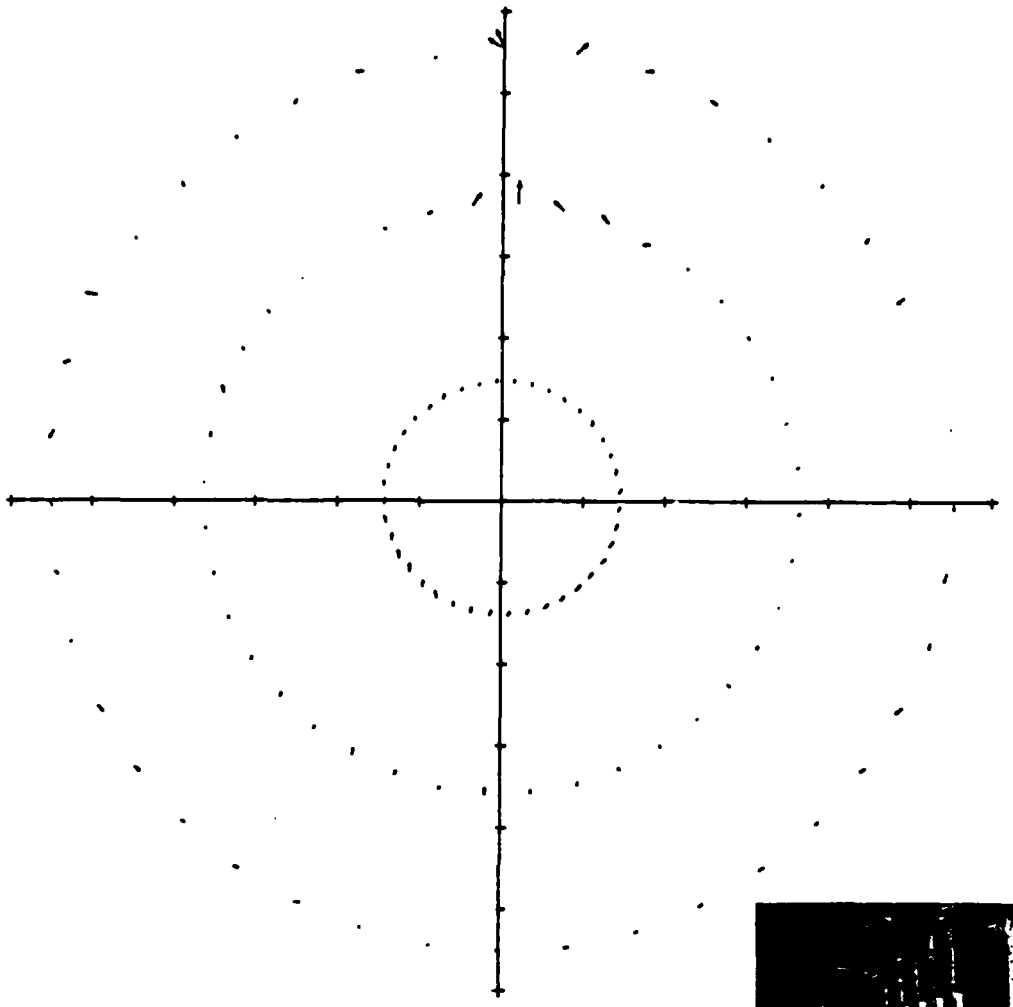

Figure 29. Steady-state flow in the plane of the test rotor, for the case of test wall number five. V_∞ = 104 fps (31.7 m/s).

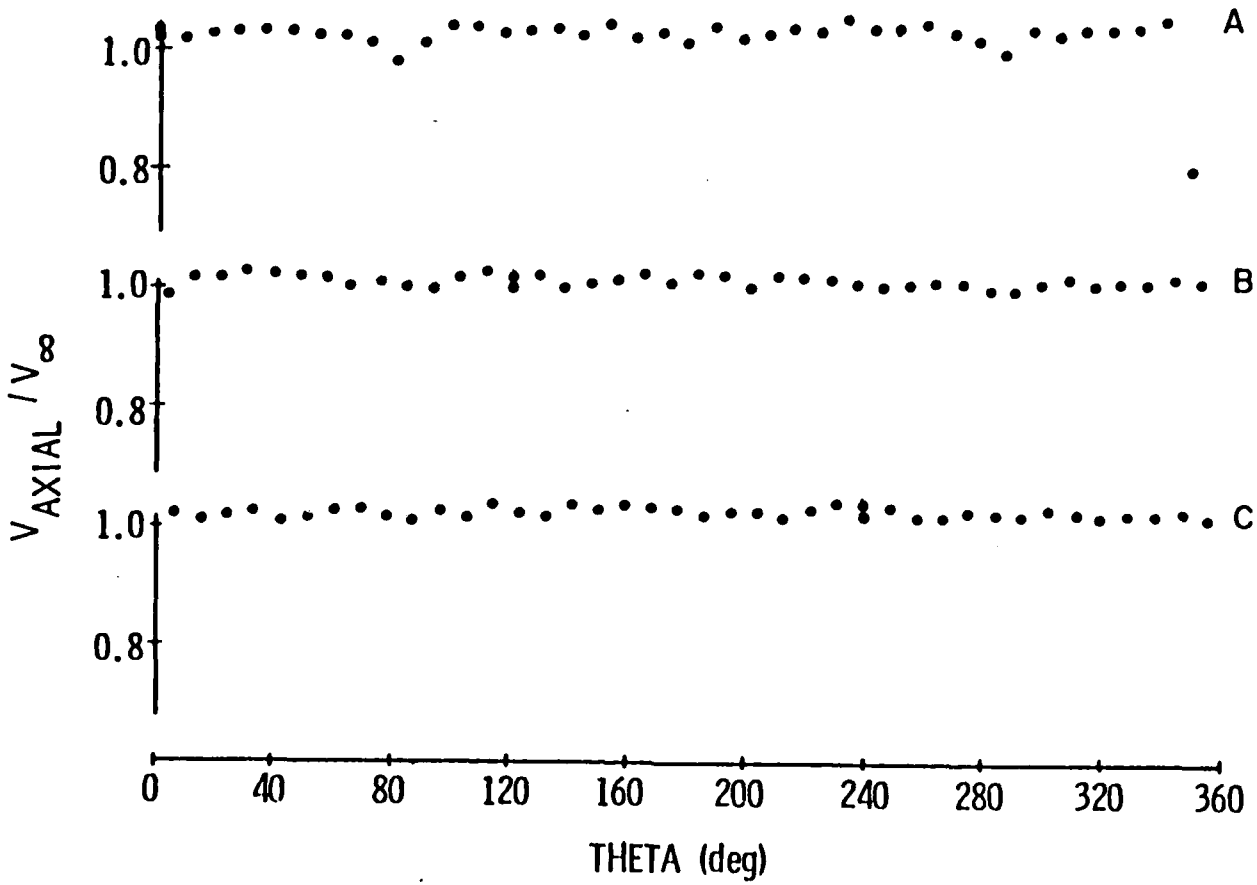

Figure 30. Steady-state axial velocities for the case of test wall number five. V_∞ = 104 fps (31.7 m/s). (A) Radius 4.15" (10.5 cm); (B) radius 2.75" (7 cm); and (C) radius 1.25" (3.2 cm).

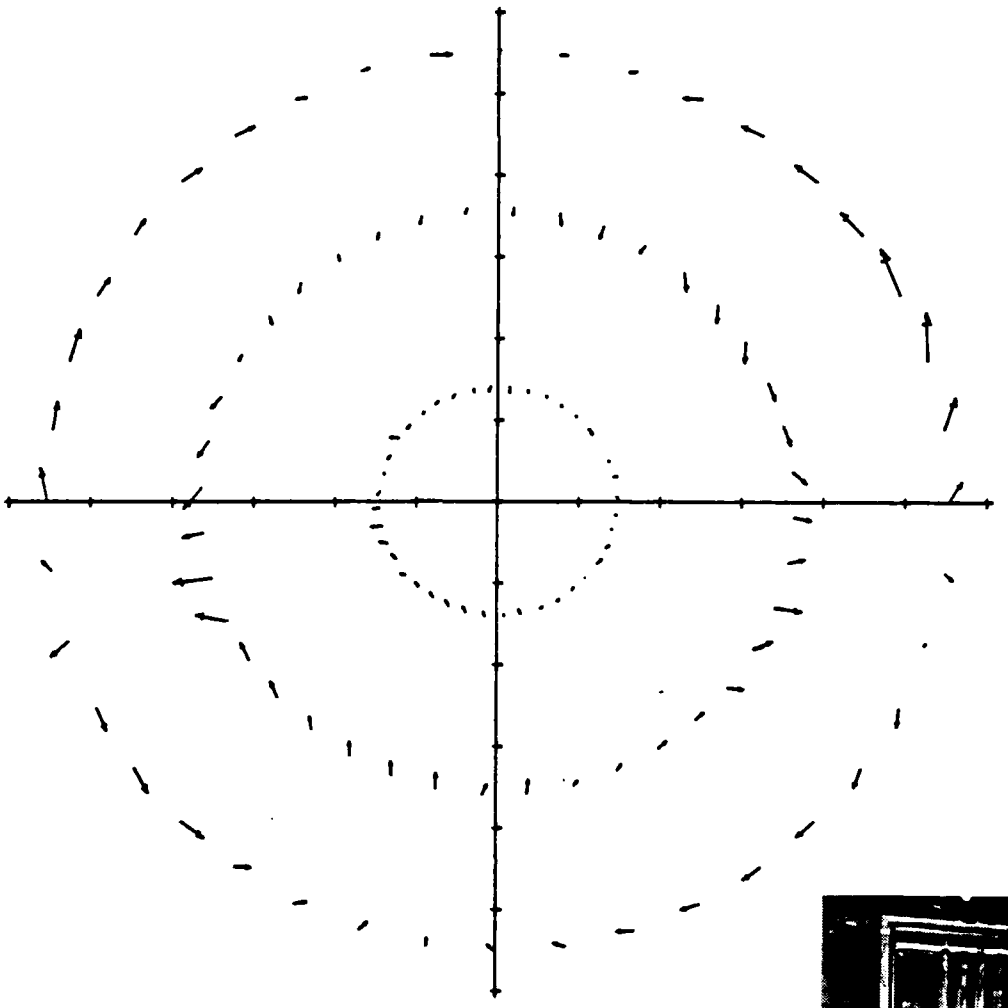

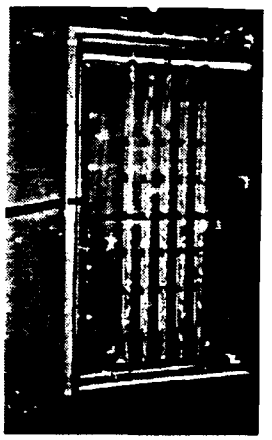

Figure 31. Steady-state flow in the plane of the test rotor, for the case of test wall number five and total top and bottom blockage. V_∞ = 98 fps (29.9 m/s).

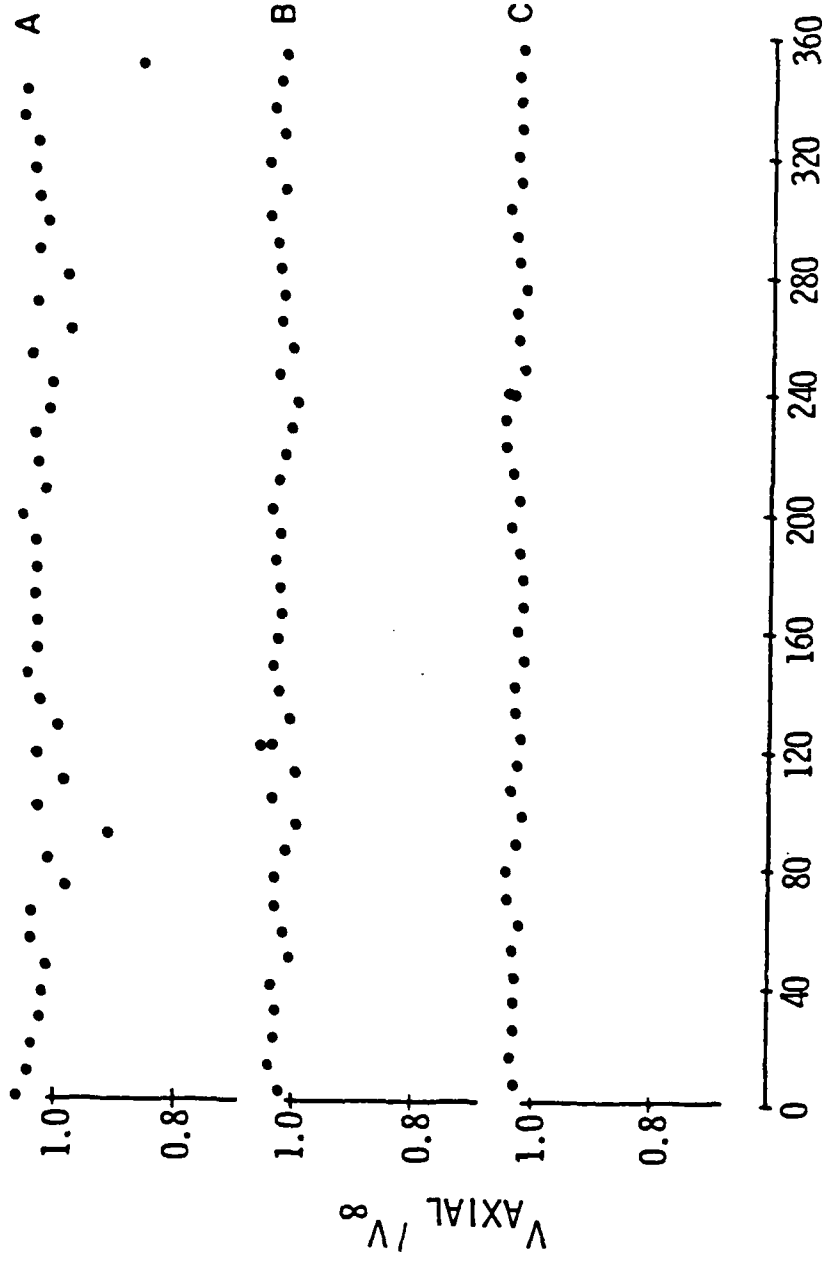

Figure 32. Steady-state axial velocities for the case of test wall number five and total top and bottom blockage. V_∞ = 98 fps (29.9 m/s). (A) Radius 4.15" (10.5 cm); (B) radius 2.75" (7 cm); and (C) radius 1.25" (3.2 cm).

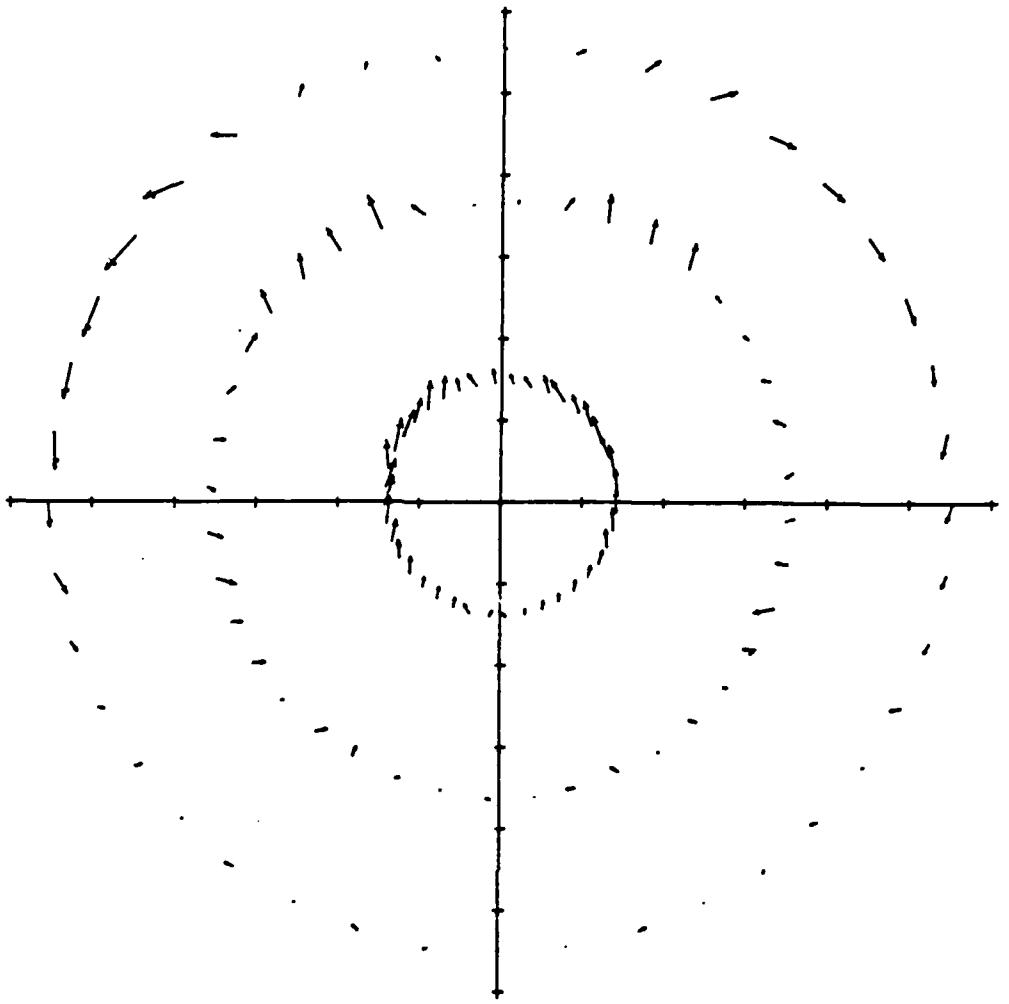

Figure 33. Steady-state flow in the plane of the test rotor, for the case of no test wall and total bottom blockage. V_∞ = 104 fps (31.7 m/s).

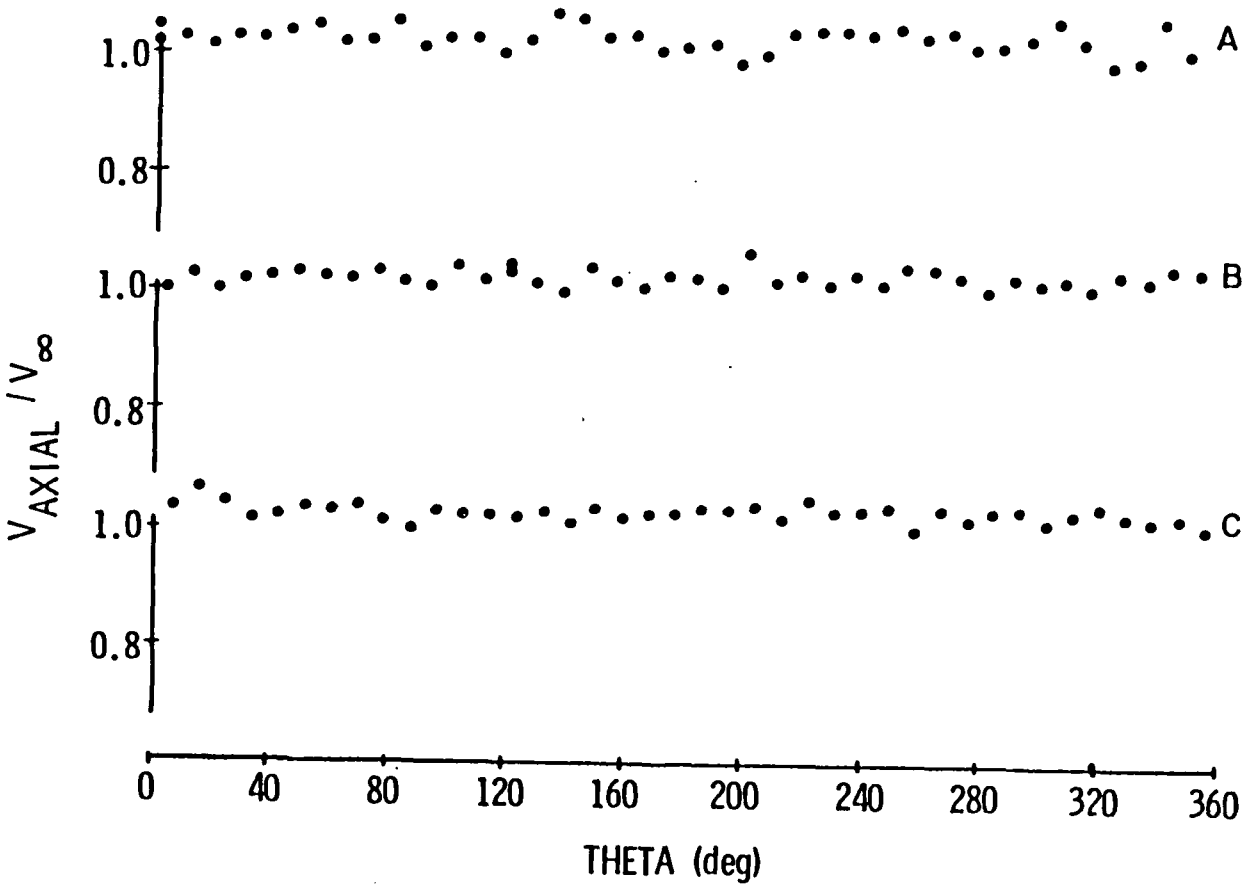

Figure 34. Steady-state axial velocities for the case of no test wall and total bottom blockage. V_∞ = 104 fps (31.7 m/s). (A) Radius 4.15" (10.5 cm); (B) radius 2.75" (7 cm); and (C) radius 1.25" (3.2 cm).

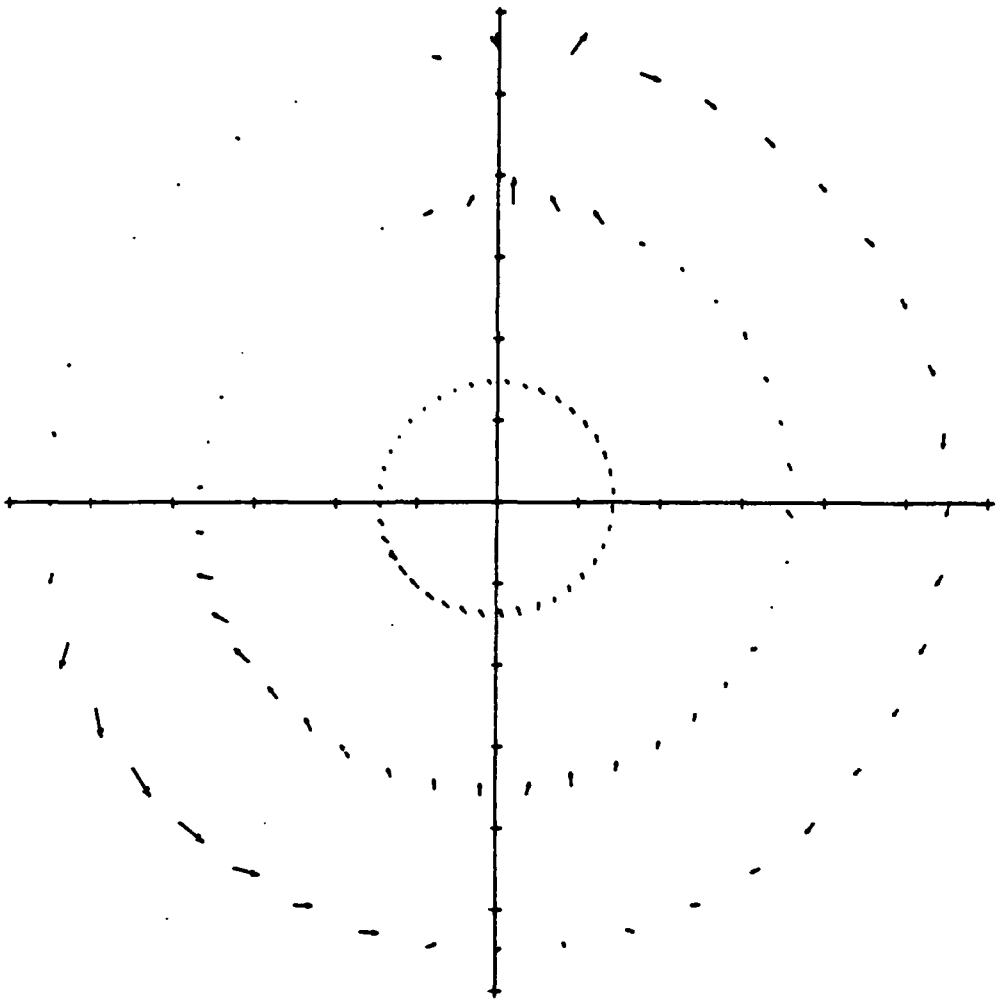

Figure 35. Steady-state flow in the plane of the test rotor, for the case of test wall number five and total bottom blockage. V_∞ = 104 fps (31.7 m/s).

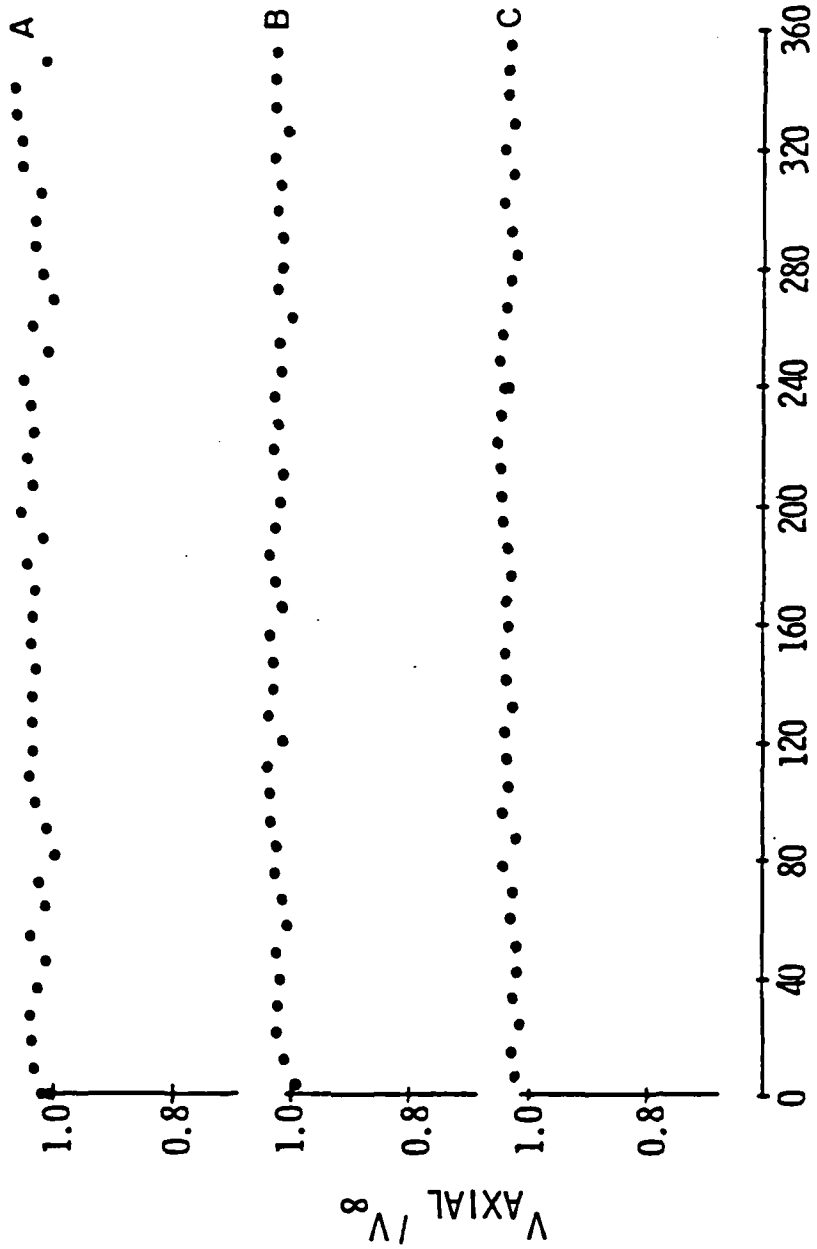

Figure 36. Steady-state axial velocities for the case of test wall number five and total bottom blockage. V_∞ = 104 fps (31.7 m/s). (A) Radius 4.15" (10.5 cm); (B) radius 2.75" (7 cm); and (C) radius 1.25" (3.2 cm).

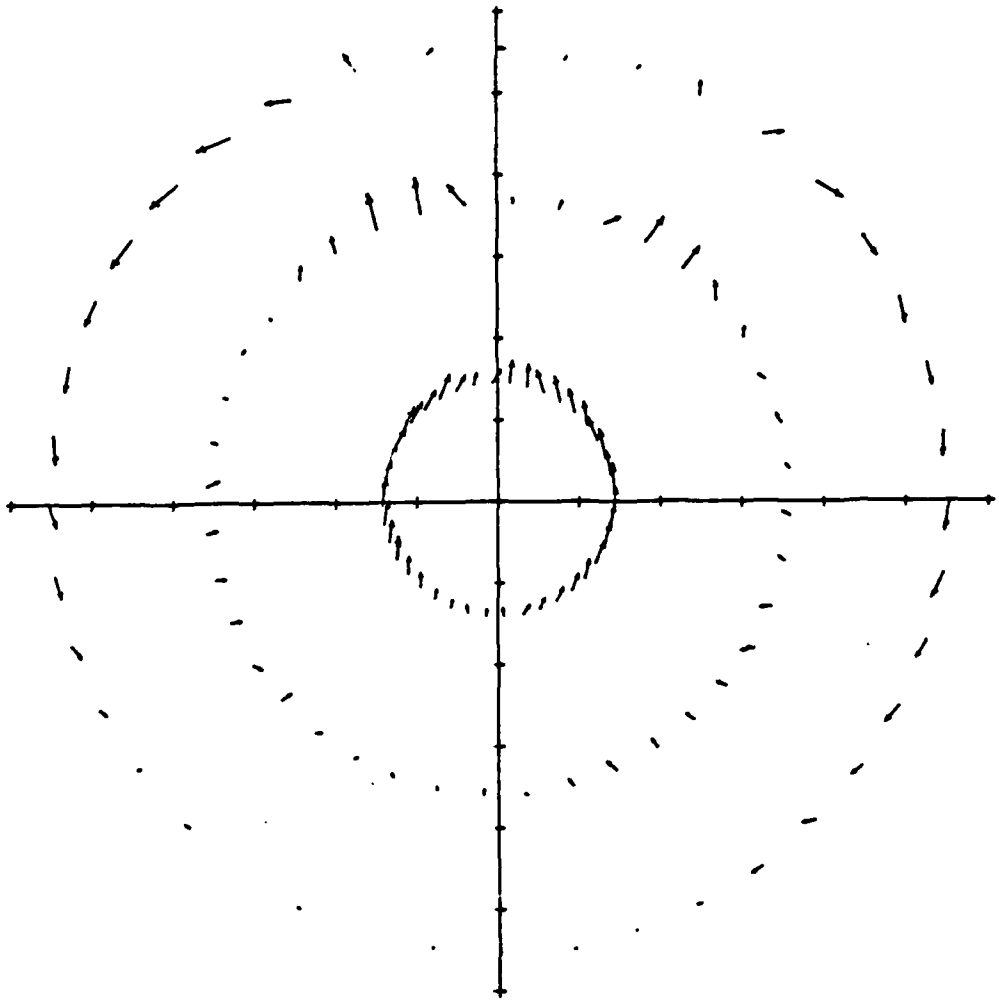

Figure 37. Steady-state flow in the plane of the test rotor, for the case of no test wall and partial top blockage. V_∞ = 97 fps (29.6 m/s).

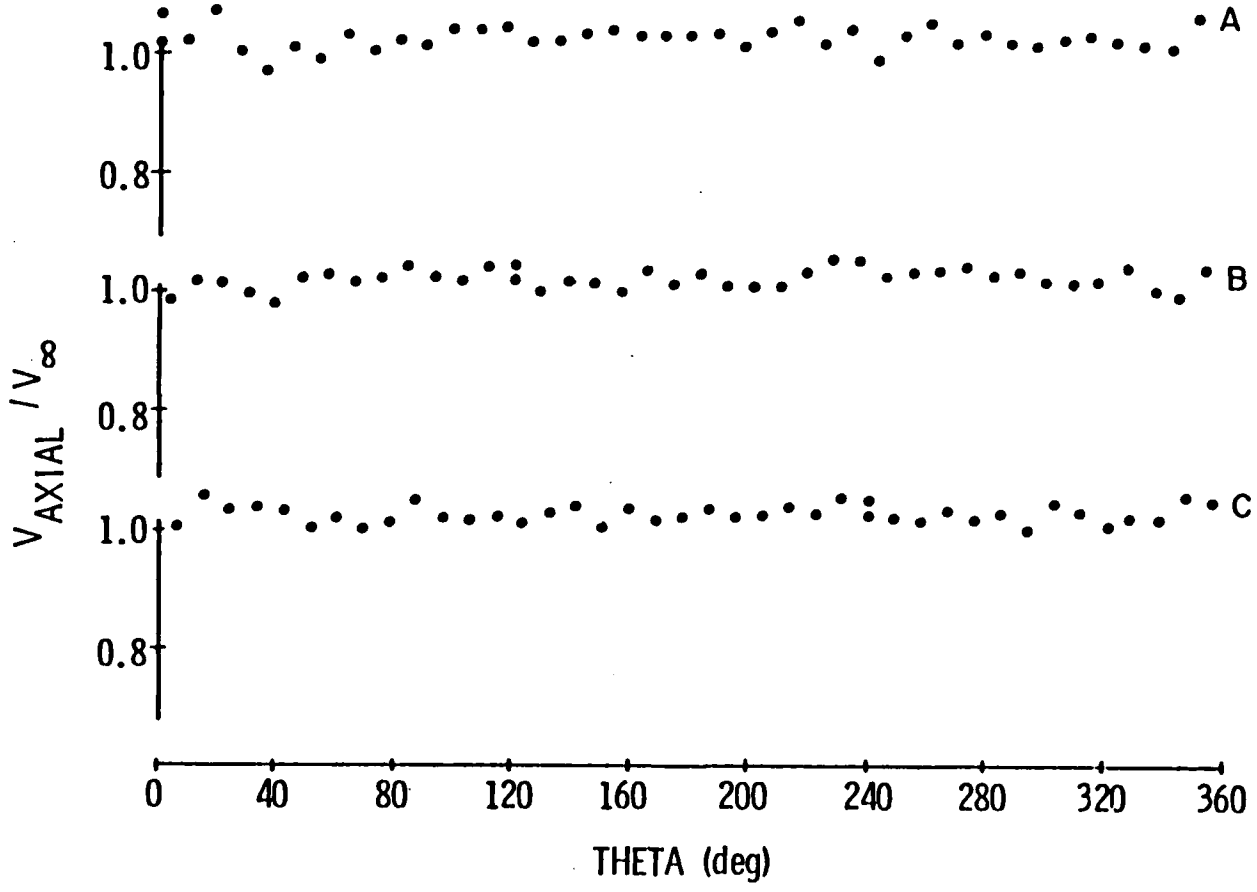

Figure 38. Steady-state axial velocities for the case of no test wall and partial top blockage. V_∞ = 97 fps (29.6 m/s). (A) Radius 4.15" (10.5 cm); (B) radius 2.75" (7 cm); and (C) radius 1.25" (3.2 cm).

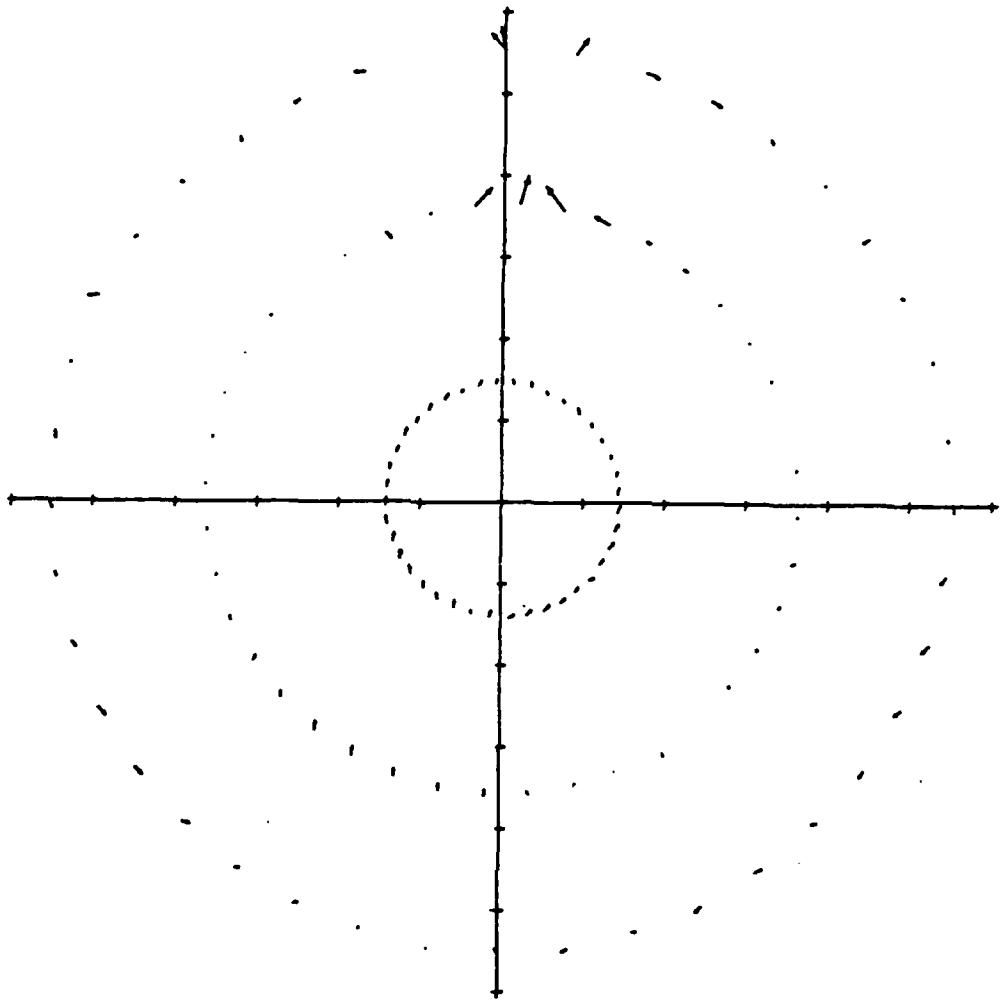

RELATIVE SCALE:
——— = $0.20V_\infty$
(MEAN VALUES SUBTRACTED OUT)

Figure 39. Steady-state flow in the plane of the test rotor, for the case of test wall number five. V_∞ = 54 fps (16.5 m/s).

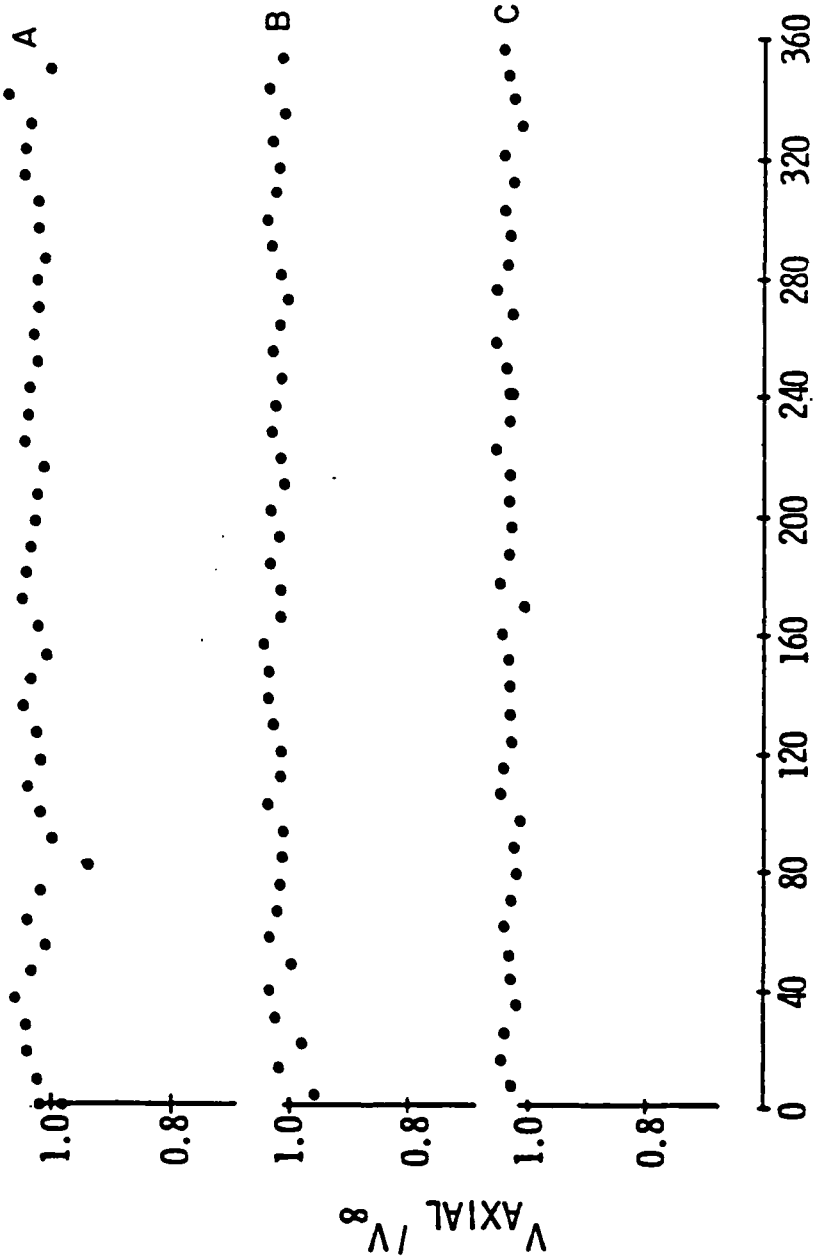

Figure 40. Steady-state axial velocities for the case of test wall number five. V_∞ = 54 fps (16.5 m/s). (A) Radius 4.15" (10.5 cm); (B) radius 2.75" (7 cm); and (C) radius 1.25" (3.2 cm).

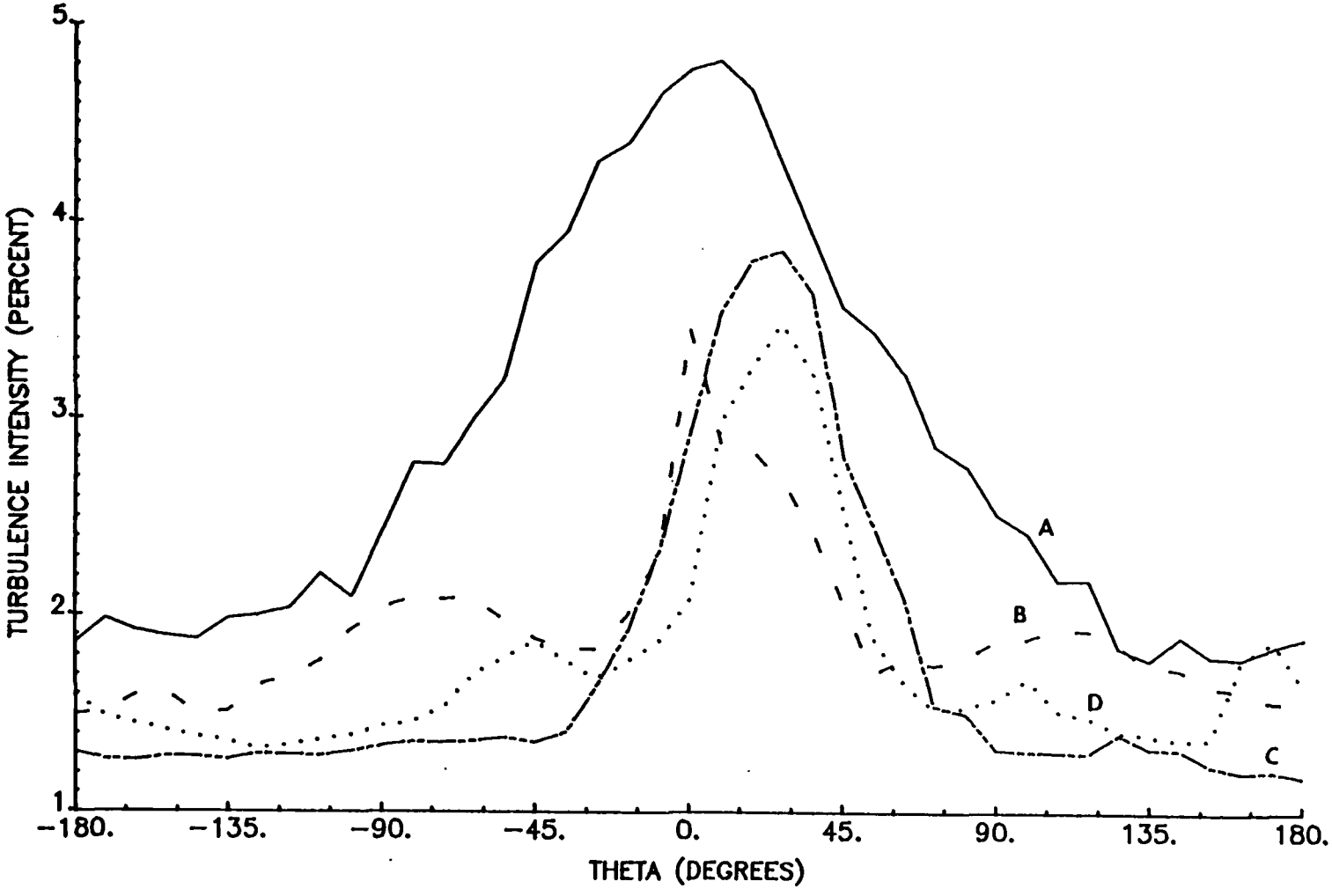

Figure 41. Axial turbulence intensity at 2 9/16" radius. (A) No test wall, V_∞ = 105 fps (32 m/s); (B) test wall number three, V_∞ = 105 fps (32 m/s); (C) test wall number four, V_∞ = 98 fps (29.9 m/s); and (D) test wall number five, V_∞ = 104 fps (31.7 m/s). 0° is top of inlet duct.

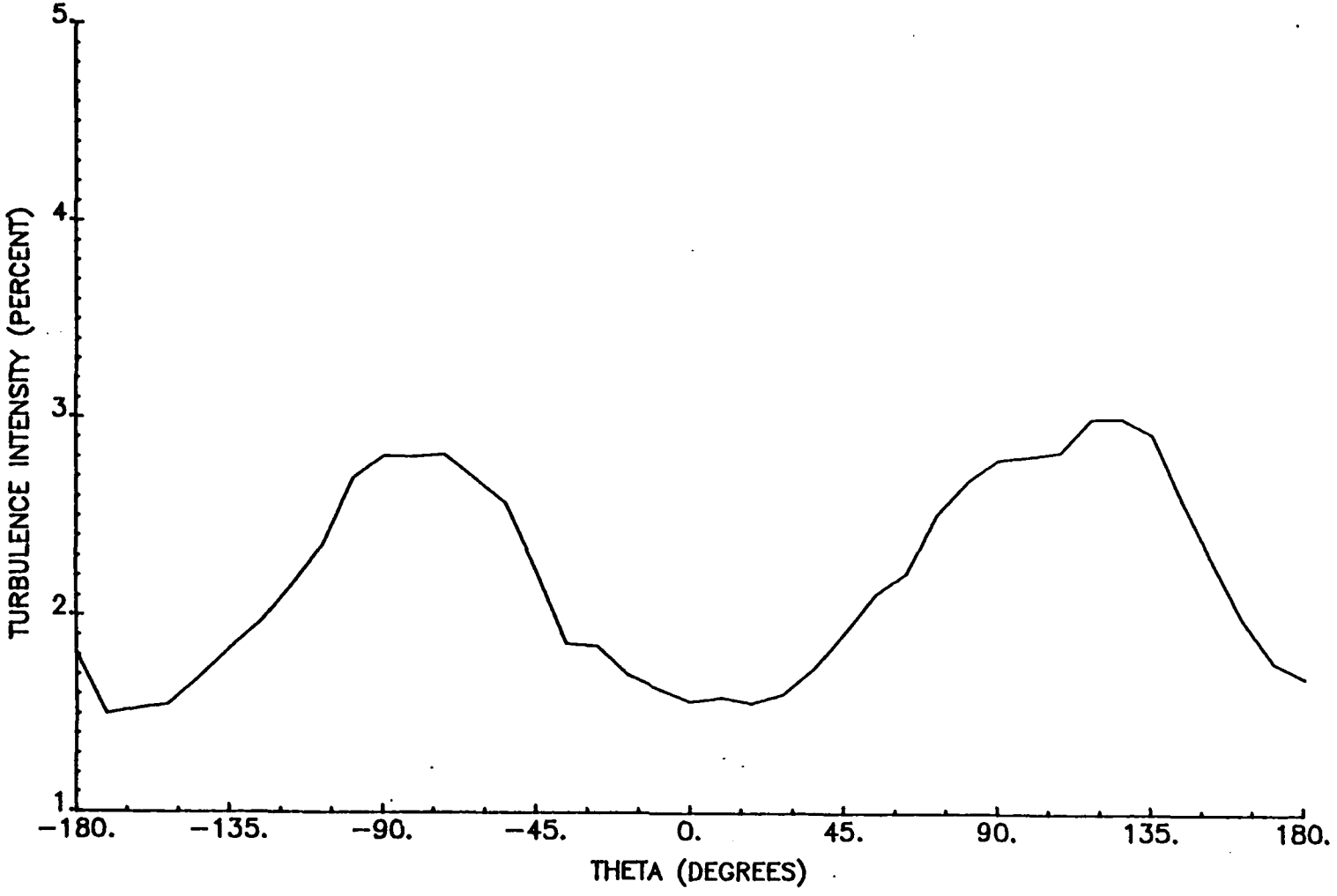

Figure 42. Axial turbulence intensity at 2 9/16" radius for the case of test wall number five and total top and bottom blockage. V_∞ = 98 fps (29.9 m/s). 0° is top of inlet duct.

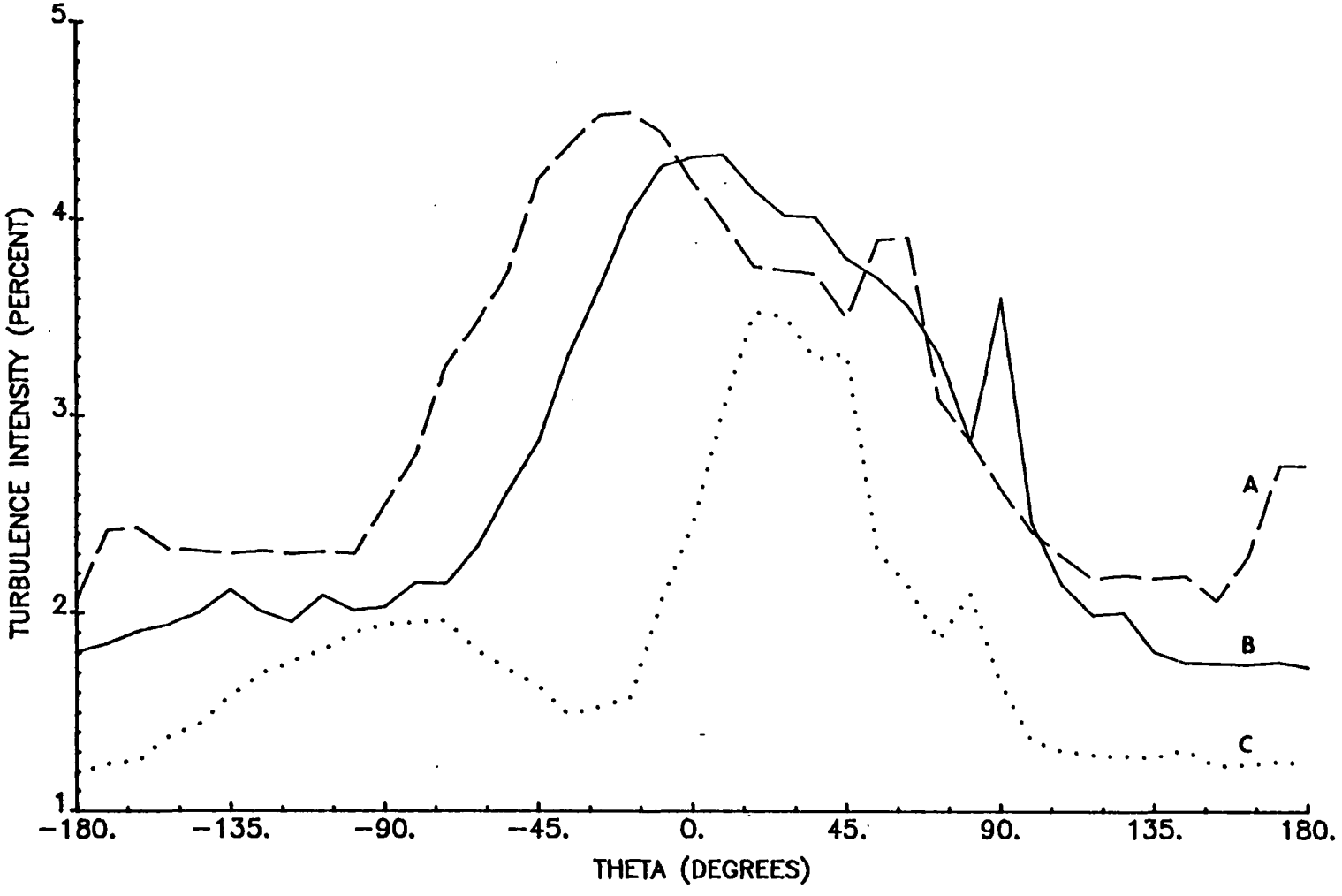

Figure 43. Axial turbulence intensity at 2 9/16" radius. (A) No test wall, total bottom blockage, V_∞ = 104 fps (31.7 m/s); (B) no test wall, partial top blockage, V_∞ = 97 fps (29.6 m/s); and (C) test wall number five, total bottom blockage, V_∞ = 104 fps (31.7 m/s). 0° is top of inlet duct.

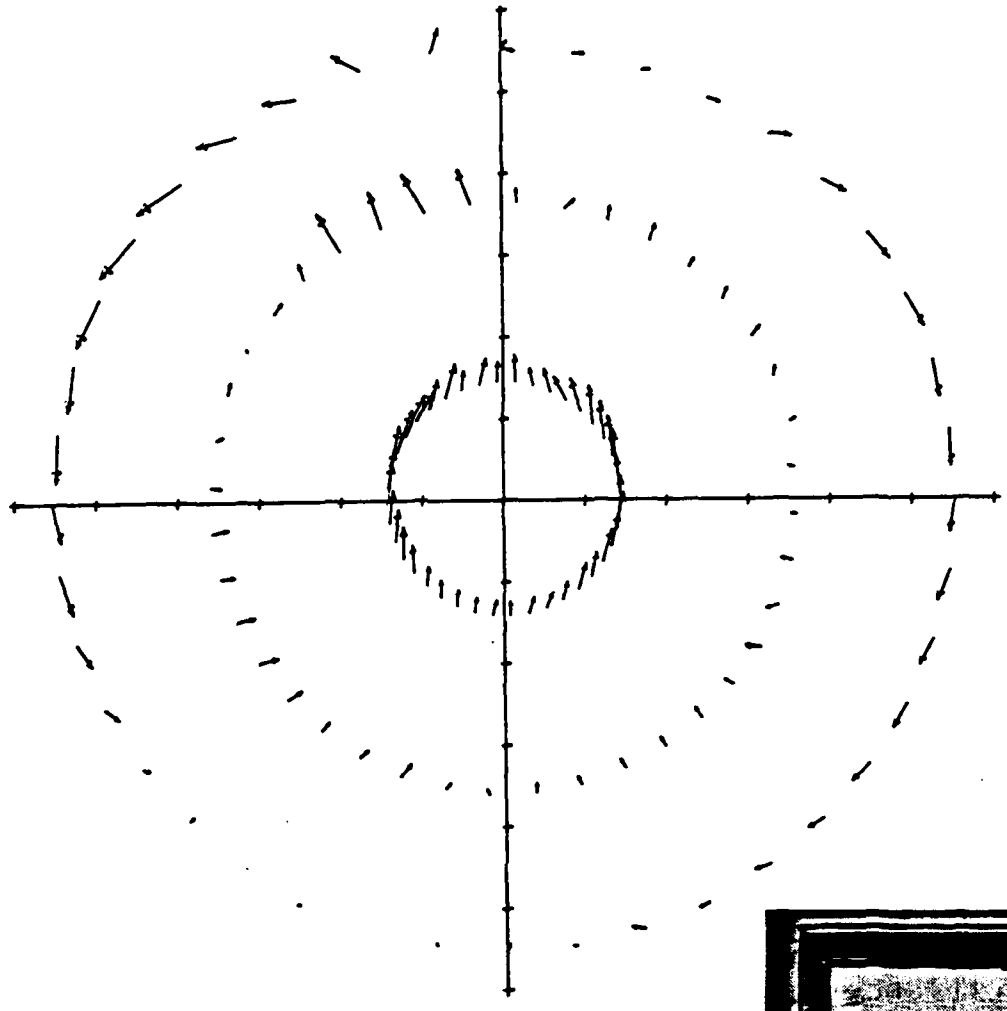

Figure 44. Steady-state flow in the plane of the test rotor, for the case of no test wall. V_∞ = 88 fps (26.8 m/s). Measurements made at the start of the final testing phase.

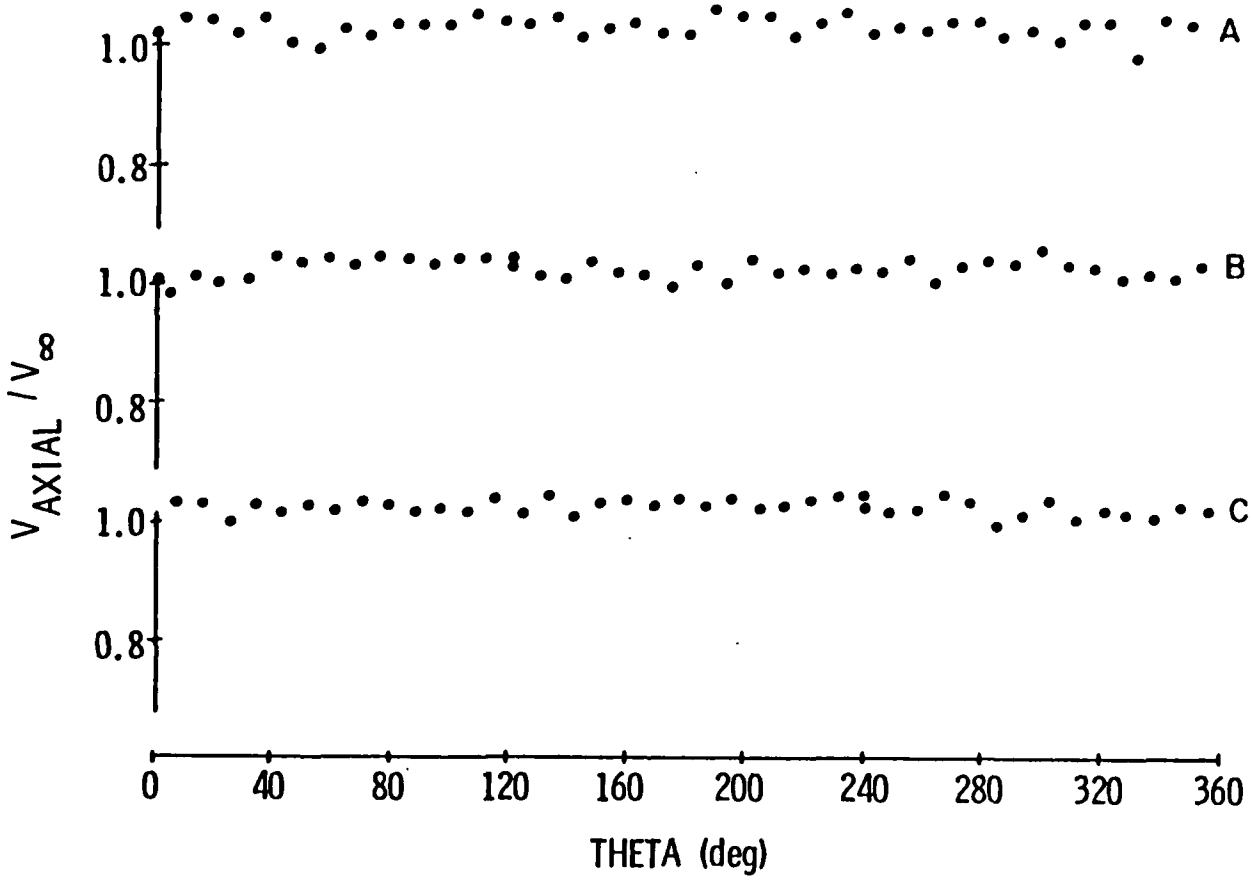

Figure 45. Steady-state axial velocities for the case of no test wall. V_∞ = 88 fps (26.8 m/s). Measurements made at the start of the final testing phase. (A) Radius 4.15" (10.5 cm); (B) radius 2.75" (7 cm); and (C) radius 1.25" (3.2 cm).

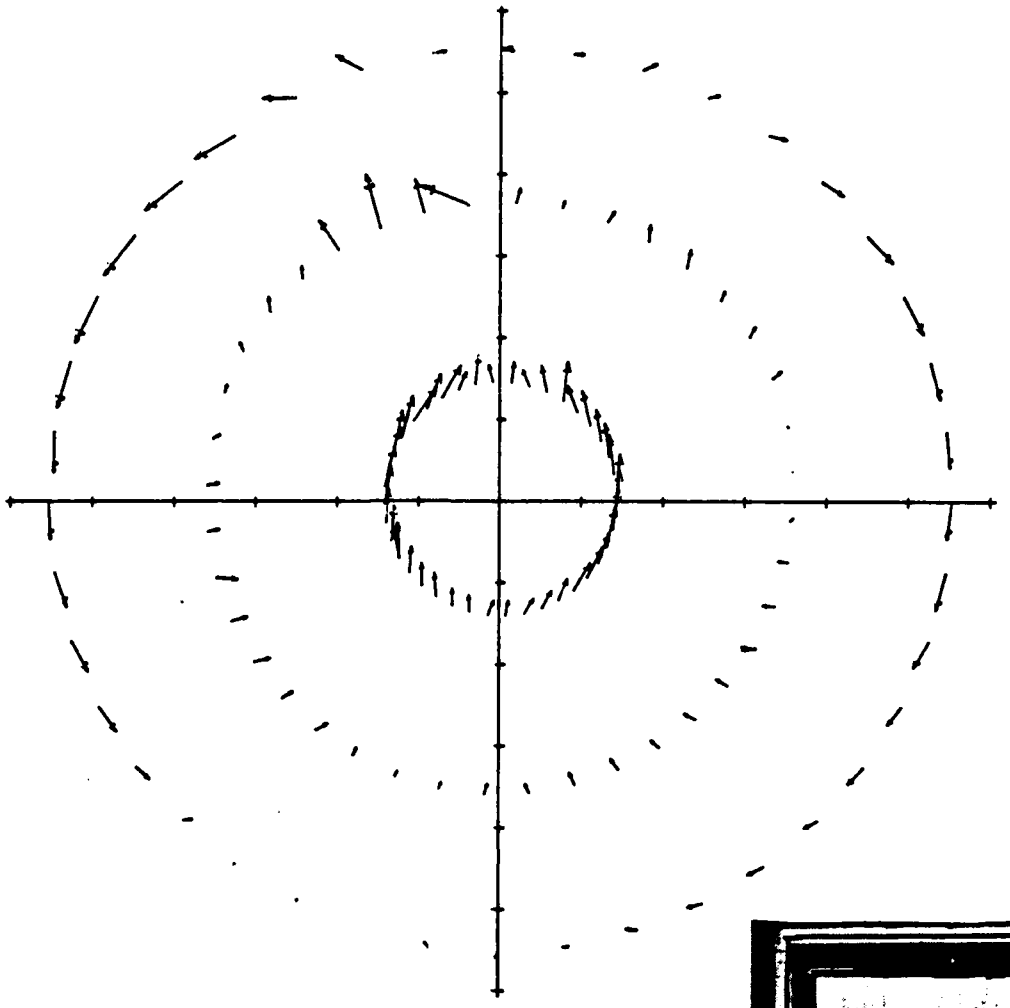

Figure 46. Steady-state flow in the plane of the test rotor, for the case of no test wall. V_∞ = 88 fps (26.8 m/s). Measurements made at the end of the final testing phase.

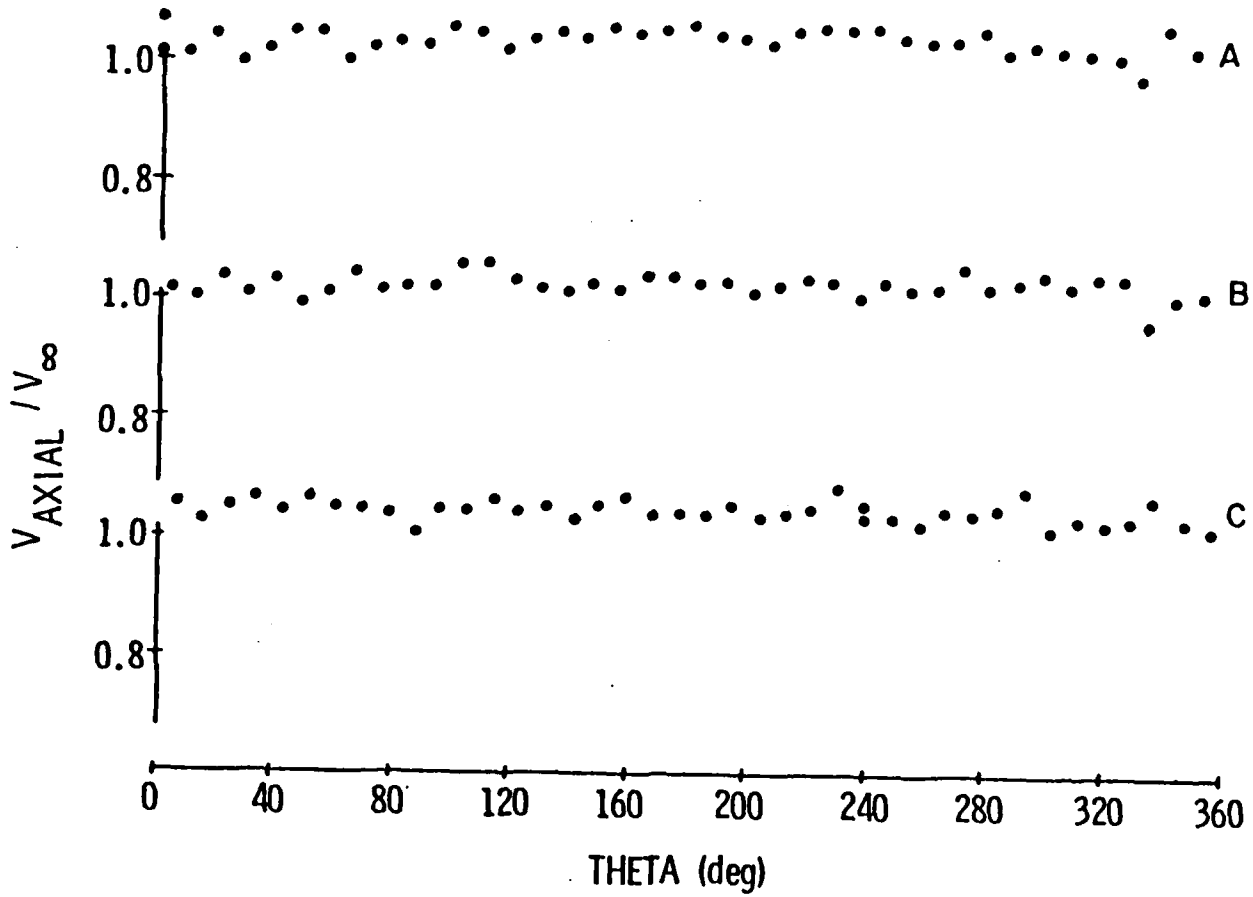

Figure 47. Steady-state axial velocities for the case of no test wall. V_∞ = 88 fps (26.8 m/s). Measurements made at the end of the final testing phase. (A) Radius 4.15" (10.5 cm); (B) radius 2.75" (7 cm); and (C) radius 1.25" (3.2 cm).

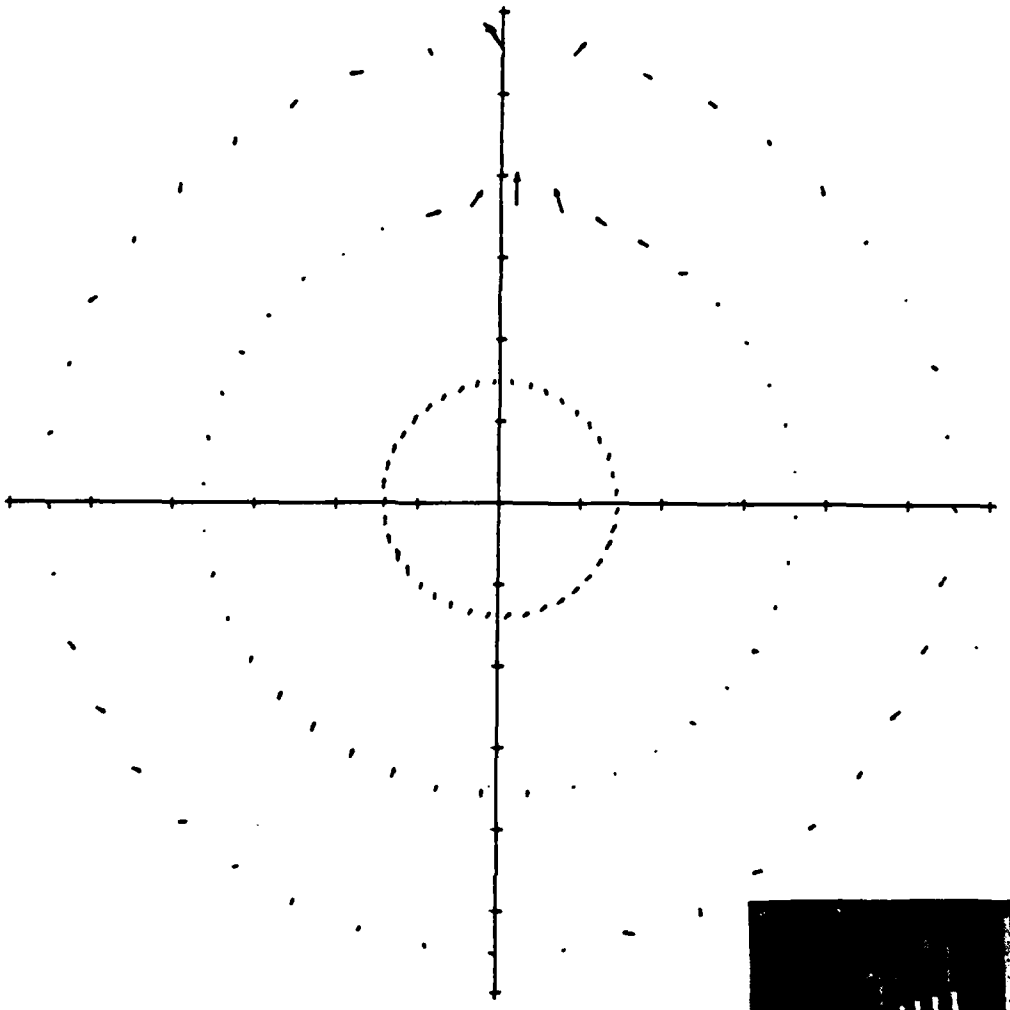

RELATIVE SCALE:
——→ = $0.20V_\infty$
(MEAN VALUES SUBTRACTED OUT)

Figure 48. Steady-state flow in the plane of the test rotor, for the case of test wall number five. V_∞ = 90 fps (27.4 m/s).

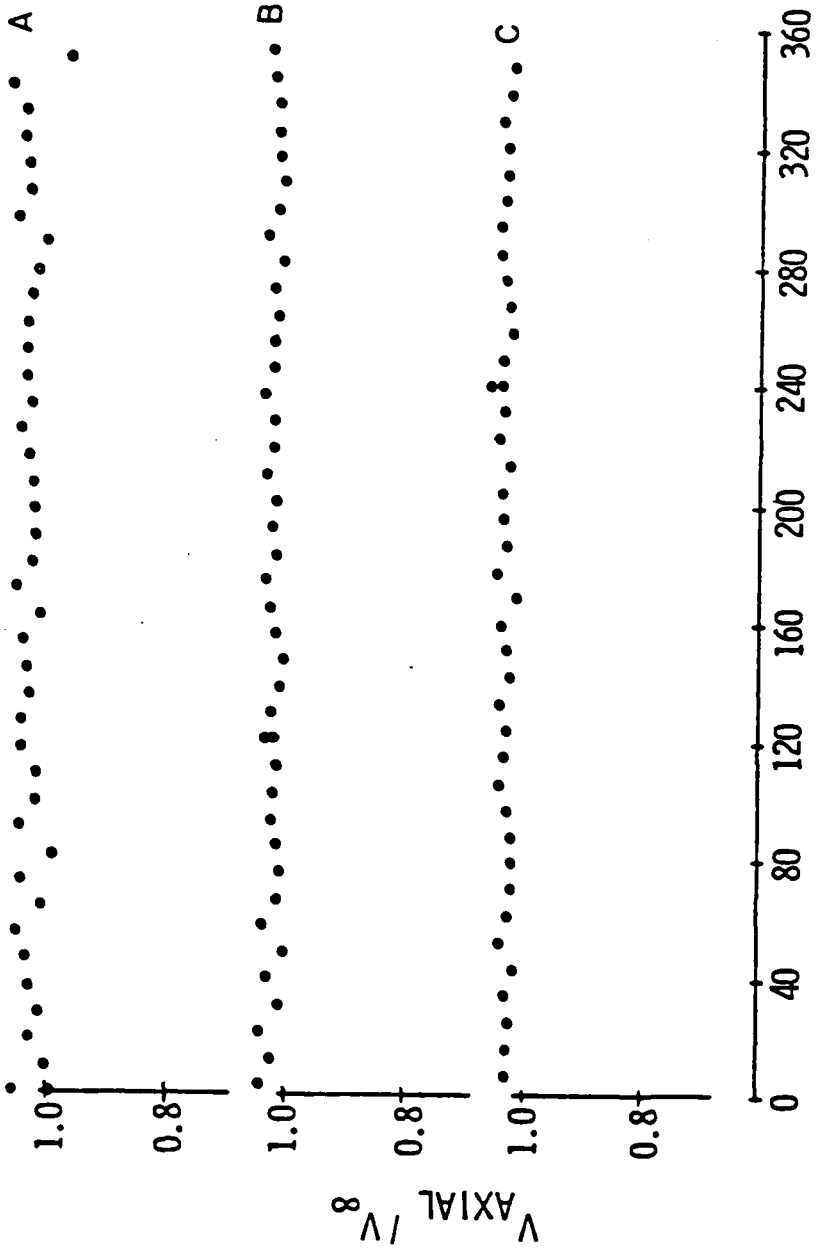

Figure 49. Steady-state axial velocities for the case of test wall number five. V_∞ = 90 fps (27.4 m/s). (A) Radius 4.15" (10.5 cm); (B) radius 2.75" (7 cm); and (C) radius 1.25" (3.2 cm).

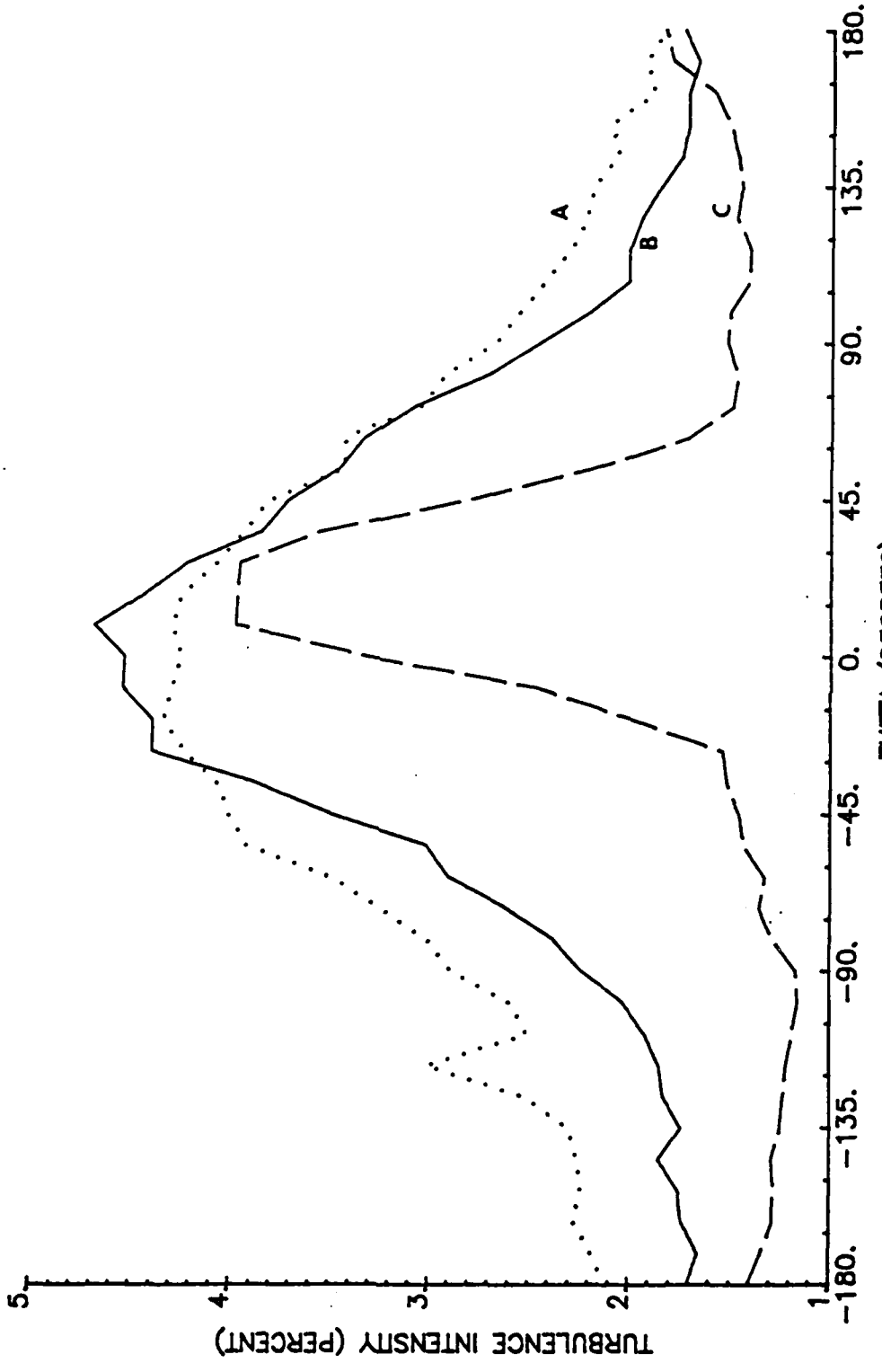

Figure 50. Axial turbulence intensity at 2 9/16" radius. (A) No test wall, V_∞ = 88 fps (26.8 m/s); (B) no test wall, V_∞ = 88 fps (26.8 m/s); and (C) test wall number five, V_∞ = 90 fps (27.4 m/s). 0° is top of inlet duct.

APPENDIX: ELECTRONIC EQUIPMENT

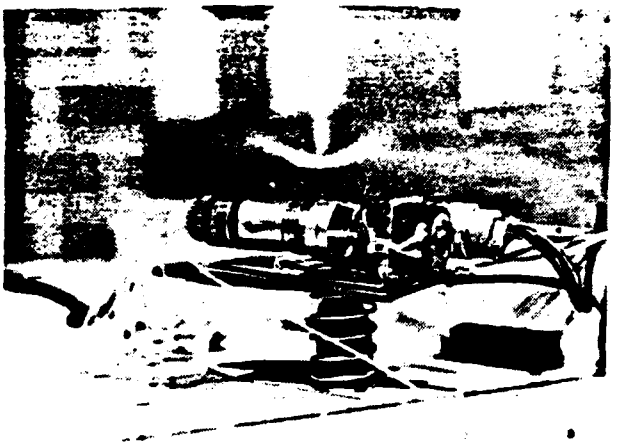

Figure A1. Scanivalve pressure-line multiplexer.

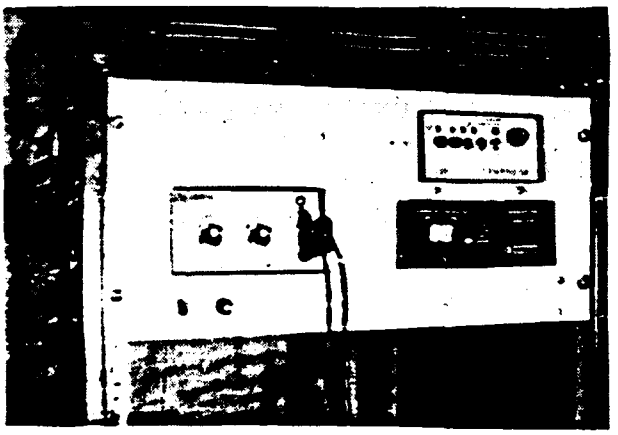

Figure A2. Validyne model CD15 carrier demodulator and pressure transducer (not visible).

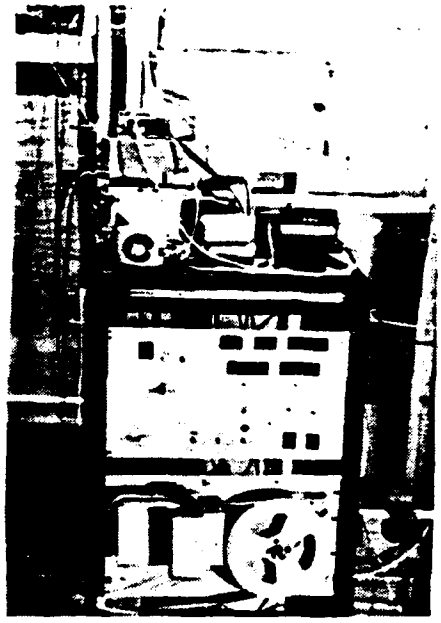

Figure A3. Digital controller/data acquisition system.

Figure A4. Hot-wire probe calibration tunnel.

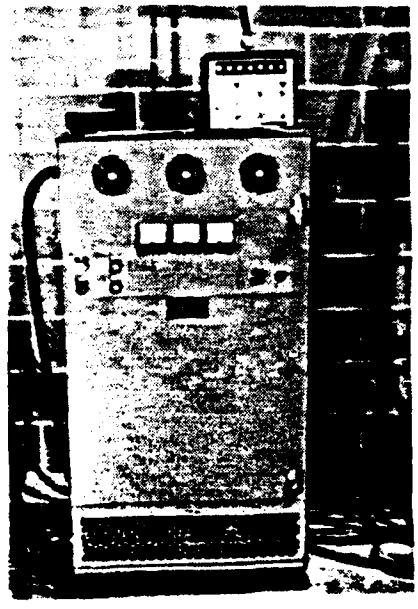

Figure A5. Borg Warner Accuspede power inverter. Speed control for fan.

DISTRIBUTION LIST FOR UNCLASSIFIED TECHNICAL MEMORANDUM FILE NO. 83-177,
by L. R. Quartararo, dated 12 October 1983

Defense Technical Information
Center
5010 Duke Street
Cameron Station
Alexandria, VA 22314
(Copies 1 through 6)

Officer in Charge
David W. Taylor Naval Ship
Research & Development Ctr.
Department of the Navy
Annapolis, MD 21402
Attention: J. W. Henry, IV
Code 2741
(Copy No. 7)

Officer in Charge
David W. Taylor Naval Ship
Research & Development Ctr.
Department of the Navy
Annapolis, MD 21402
Attention: J. V. Pierpoint
Code 4223.3
(Copy No. 8)

Commander
David W. Taylor Naval Ship
Research & Development Ctr.
Department of the Navy
Bethesda, MD 20084
Attention: F. S. Archibald
Code 1942
(Copy No. 9)

Commander
David W. Taylor Naval Ship
Research & Development Ctr.
Department of the Navy
Bethesda, MD 20084
Attention: W. K. Blake
Code 1905
(Copy No. 10)

Commander
David W. Taylor Naval Ship
Research & Development Ctr.
Department of the Navy
Bethesda, MD 20084
Attention: M. M. Sevik
Code 19
(Copy No. 11)

Commander
Naval Sea Systems Command
Department of the Navy
Washington, DC 20362
Attention: A. R. Paladino
Code 55N
(Copy No. 12)

Commander
Naval Sea Systems Command
Department of the Navy
Washington, DC 20362
Attention: T. E. Peirce
Code 63R31
(Copy No. 13)

Commanding Officer
Naval Underwater Systems Ctr.
Department of the Navy
Newport, RI 02840
Attention: D. J. Goodrich
Code 36301
(Copy No. 14)

Commanding Officer
Naval Underwater Systems Ctr.
Department of the Navy
Newport, RI 02840
Attention: R. J. Kittredge
Code 3542
(Copy No. 15)

Commanding Officer
Naval Underwater Systems Ctr.
Department of the Navy
Newport, RI 02840
Attention: B. J. Myers
Code 3631
(Copy No. 16)

Commanding Officer
Naval Underwater Systems Ctr.
Department of the Navy
Newport, RI 02840
Attention: R. H. Nadolink
Code 3634
(Copy No. 17)

DISTRIBUTION LIST FOR UNCLASSIFIED TECHNICAL MEMORANDUM FILE NO. 83-177,
by L. R. Quartararo, dated 12 October 1983
[continuation]

Office of Naval Research
800 North Quincy Street
Department of the Navy
Arlington, VA 22217
Attention: M. M. Reischman
Code 432
(Copy No. 18)

Office of Naval Research
800 North Quincy Street
Department of the Navy
Arlington, VA 22217
Attention: R. E. Whitehead
Code 432F
(Copy No. 19)

Dr. R. E. A. Arndt
St. Anthony Falls Hydraulic Lab
The University of Minnesota
Mississippi River at 3rd Ave., S.E.
Minneapolis, MN 55414
(Copy No. 20)

Dr. R. J. Hansen
Naval Research Laboratory
Marine Technical Division
Washington, DC 20390
(Copy No. 21)

Dr. W. W. Lang
IBM Corporation
Acoustics Laboratory
Post Office Box 390
Poughkeepsie, NY 12602
(Copy No. 22)

Professor P. Leehey
Department of Ocean Engineering
Massachusetts Institute of
Technology
77 Massachusetts Avenue
Cambridge, MA 02139
(Copy No. 23)

Professor J. L. Lumley
Sibley School of Mechanical &
Aeronautical Engineering
Upson Hall
Cornell University
Ithaca, NY 14850
(Copy No. 24)

Dr. L. Maestrello
NASA Langley Research Ctr.
Hampton, VA 22665
(Copy No. 25)

Mr. G. Maling
IBM Corporation
Acoustics Laboratory
Post Office Box 390
Poughkeepsie, NY 12602
(Copy No. 26)

Mr. L. R. Quartararo
Stone & Webster Engineering
Corporation
Post Office Box 2325
Boston, MA 02107
(Copies 27 and 28)

Mr. R. Weis
IBM Corporation
Acoustics Laboratory
Post Office Box 390
Poughkeepsie, NY 12602
(Copy No. 29)

Mr. D. Yeager
IBM Corporation
Acoustics Laboratory
Post Office Box 390
Poughkeepsie, NY 12602
(Copy No. 30)

Director
Applied Research Laboratory
The Pennsylvania State University
Post Office Box 30
State College, PA 16804
Attention: G. B. Gurney
(Copy No. 31)

DISTRIBUTION LIST FOR UNCLASSIFIED TECHNICAL MEMORANDUM FILE NO. 83-177,
by L. R. Quartararo, dated 12 October 1983
[continuation]

Director
Applied Research Laboratory
The Pennsylvania State University
Post Office Box 30
State College, PA 16804
Attention: R. E. Henderson
(Copy No. 32)

Director
Applied Research Laboratory
The Pennsylvania State University
Post Office Box 30
State College, PA 16804
Attention: L. R. Hettche
(Copy No. 33)

Director
Applied Research Laboratory
The Pennsylvania State University
Post Office Box 30
State College, PA 16804
Attention: G. C. Lauchle
(Copy No. 34)

Director
Applied Research Laboratory
The Pennsylvania State University
Post Office Box 30
State College, PA 16804
Attention: B. R. Parkin
(Copy No. 35)

Director
Applied Research Laboratory
The Pennsylvania State University
Post Office Box 30
State College, PA 16804
Attention: J. H. Prout
(Copy No. 36)

Director
Applied Research Laboratory
The Pennsylvania State University
Post Office Box 30
State College, PA 16804
Attention: F. E. Smith
(Copy No. 37)

Director
Applied Research Laboratory
The Pennsylvania State University
Post Office Box 30
State College, PA 16804
Attention: R. Stern
(Copy No. 38)

Director
Applied Research Laboratory
The Pennsylvania State University
Post Office Box 30
State College, PA 16804
Attention: A. D. Stuart
(Copy No. 39)

Director
Applied Research Laboratory
The Pennsylvania State University
Post Office Box 30
State College, PA 16804
Attention: D. E. Thompson
(Copy No. 40)

Director
Applied Research Laboratory
The Pennsylvania State University
Post Office Box 30
State College, PA 16804
Attention: J. Tichy
(Copy No. 41)

Director
Applied Research Laboratory
The Pennsylvania State University
Post Office Box 30
State College, PA 16804
Attention: A. L. Treaster
(Copy No. 42)

Director
Applied Research Laboratory
The Pennsylvania State University
Post Office Box 30
State College, PA 16804
Attention: GTWT Files
(Copy No. 43)

DISTRIBUTION LIST FOR UNCLASSIFIED TECHNICAL MEMORANDUM FILE NO. 83-177,
by L. R. Quartararo, dated 12 October 1983
[continuation]

Director
Applied Research Laboratory
The Pennsylvania State University
Post Office Box 30
State College, PA 16804
Attention: ARL/PSU Library
(Copy No. 44)

END

FILMED

1-85

DTIC